

NASA Contractor Report 172316

(NASA-CR-172316) NEW COHERENT OPTICAL
TECHNIQUES FOR NATIONAL TRANSONIC WIND
TUNNEL FACILITY Final Report, 1 May 1982 -
1 May 1983 (Carnegie-Mellon Univ.) 76 p
LIMIT GOVT.+CONTR.

X84-10259

E3/74 Unclass
18954

NEW COHERENT OPTICAL TECHNIQUES FOR NATIONAL
TRANSONIC WIND TUNNEL FACILITY

David Casasent

CARNEGIE-MELLON UNIVERSITY
Pittsburgh, Pennsylvania 15213

Grant NAG1-265
March 1984

FOR U.S. GOVERNMENT AGENCIES
AND THEIR CONTRACTORS ONLY

COPY CONTROL NO. _____ 3

NASA

National Aeronautics and
Space Administration

Langley Research Center
Hampton, Virginia 23665



ABSTRACT

The goal of this one year study was to survey the use of optical data processing techniques for distortion-parameter estimation in the National Transonic Facility and to assess, quantify and compare various methods to determine which are best for this specific application. The conventional nondestructive testing techniques studied included interferometry, moire and speckle methods. From these, we find projection moire using fringe multiplication to provide sufficient accuracy and to be a most attractive approach for this application. Several advanced moire techniques for future research are also described. We also investigated several correlation techniques: space-variant processing, stereo correlation and autocorrelation shape analysis. Stereo correlation is found to have sufficient accuracy and new modified stereo correlation techniques for this application which are most appropriate are described. Autocorrelation shape analysis is a quite unique approach to distortion-parameter estimation. Finally, several optical feature extraction techniques were considered. These included Fourier transform coefficients, wedge ring detector-sampled Fourier transform data and moment features. In all cases, each feature is optically-generated and a digital post-processor is used to determine the target's distortion parameters. We find: projection moire (with fringe multiplication), wedge ring detector: Fourier transform plane analysis and moment-based optically-generated features to be the most attractive techniques that merit further attention for this application.

TABLE OF CONTENTS

	<u>PAGE</u>
ABSTRACT-----	i
1. INTRODUCTION-----	1
1.1 PROBLEM DEFINITION-----	1
1.2 WIND TUNNEL MODEL SAMPLE TESTS-----	4
1.3 SCOPE OF REPORT-----	7
2. INTERFEROMETRIC, MOIRE AND SPECKLE TECHNIQUES-----	9
2.1 INTRODUCTION-----	9
2.2 OVERVIEW-----	9
2.3 PROJECTION MOIRE AND FRINGE MULTIPLICATION-----	15
2.4 ADVANCED APPROACHES AND SUMMARY-----	22
3. CORRELATION AND OTHER TECHNIQUES-----	24
3.1 INTRODUCTION-----	24
3.2 TURBULENCE AND VIBRATIONS-----	24
3.3 SPACE-VARIANT IMAGE PROCESSING-----	25
3.4 STEREO CORRELATION TECHNIQUES-----	27
3.5 AUTOCORRELATION SHAPE ANALYSIS-----	35
3.6 SUMMARY AND CONCLUSION-----	40
4. OPTICALLY-GENERATED PATTERN FEATURES FOR DISTORTION-PARAMETER ESTIMATIONS-----	41
4.1 INTRODUCTION-----	41
4.2 PATTERNS USED-----	43
4.3 FOURIER COEFFICIENT FEATURE SPACE-----	45
4.4 WRD-SAMPLED FOURIER COEFFICIENT FEATURE SPACE CONCEPT-----	51
4.5 INITIAL ISSUES IN THE ANALYSIS OF A WRD/FOURIER-COEFFICIENT FEATURE SPACE-----	54
4.6 OPTICAL MOMENT FEATURE SPACE SYNTHESIS-----	55
4.7 MOMENT PROCESSOR FOR DISTORTION-PARAMETER ESTIMATION (COMPONENT REQUIREMENT)-----	57
4.8 SUMMARY AND CONCLUSIONS-----	62
5. SUMMARY, HIGHLIGHTS AND FUTURE WORK-----	64
5.1 SUMMARY-----	64
5.2 HIGHLIGHTS-----	66
5.3 FUTURE WORK-----	68
REFERENCES-----	70
LIST OF TABLES-----	iii
LIST OF FIGURES-----	iii

LIST OF TABLES

	<u>PAGE</u>
1.1 Initial New Coherent Optical Techniques Considered-----	4
1.2 Additional Coherent Optical Techniques Considered-----	4
2.1 Interferometric and Other Techniques Considered-----	10
4.1 Experimental Data Obtained Using Fourier Coefficient Measurements---	48

LIST OF FIGURES

	<u>PAGE</u>
1.1 Photographs of Sample Using White Light Source and Using Laser Source-----	6
2.1 Optical Setup for Projection Moire Surface Metrology Tests-----	16
2.2 Image of Original Grating Pattern on Object-----	18
2.3 Moire Image (Object Contour More Apparent)-----	18
2.4 Examples of Fringe Multiplication for Improved Accuracy Projection Moire Contouring-----	21
3.1 Schematic Diagram of a System that can Produce Stereo-Pairs of Photographs-----	29
3.2 Schematic Diagram of an Optical Frequency Plane Correlator-----	32
3.3 Cross-Sectional Scans of the Autocorrelations of an Undistorted and Distorted Input Pattern-----	37
4.1 Simplified Grating Pattern Inputs Used in Analysis-----	43
4.2 Simplified Schematic of the Scaling Fourier Transform Processing System-----	46
4.3 Partial Fourier Transform Plane Pattern Obtained on the System of Figure 4.2 for Two Distorted Grating Patterns-----	49
4.4 Selected Cross-Sectional Scans of the Fourier Transform Pattern Obtained on the System of Figure 4.2 With and Without Scale Distortions in the Input Object Grating Pattern-----	49

LIST OF FIGURES (CONTINUED):

	<u>PAGE</u>
4.5 Pictorial Diagram of the Wedge Ring Detector-Sampling Unit Proposed for Dimensionality Reduction and Distortion-Parameter Estimation-----	52
4.6 Schematic Diagram of a Parallel Coherent Optical Processor to Compute the Moments of an Input Image-----	57

Final Technical Report
"New Coherent Optical Techniques for National
Transonic Wind Tunnel Facility"

David Casasent
Carnegie-Mellon University
Department of Electrical Engineering
Pittsburgh, Pennsylvania 15213

1. INTRODUCTION

1.1 PROBLEM DEFINITION

The new National Transonic Wind Tunnel Facility (NTF) at NASA Langley produces much larger model deformations due to increased aerodynamic loading and temperature thus requiring advanced deformation measurement techniques. A spatially continuous real-time description of the model deformations is desired, although deformations at about 50-100 discrete points or regions on the model surface at discrete times are sufficient. It is preferable that no patterns be placed on the model as this can disturb its performance under NTF testing. The model ($0.9 \times 0.9\text{m}^2$) can exhibit deflections of 7.62cm which must be measured to an accuracy of $\pm 64\mu\text{m}$.

Other features that arise in the NTF are the large dynamic density variations present in the test chamber (due to the strong turbulence involved) and to the very smooth model surface. The density variations cause differences in the optical path length for different parts of the medium. The smooth specular surface of the model may allow light to be reflected only in narrow angular directions rather than in all directions (as would occur with a diffuse surface). Due to the physical constraints of the NTF, cameras or other viewing devices

used in the measurement system can be mounted only in the floor or ceiling of the wind tunnel. This excludes the possibility of using side-on viewing angles. It is assumed that the measurement system will be subjected to significant vibration levels and that isolation or some form of compensation will be required. This is discussed briefly later.

The purpose of this project was to investigate new coherent optical processing techniques for this application. The ten techniques originally proposed and considered are noted in Table 1.1.

Since the Fourier transform operation is directly realized in a coherent optical system, the presence and value of the Fourier coefficients is an obvious initial choice. Sampling of the Fourier transform plane with a wedge ring detector (WRD) is a potential useful technique. The wedge information should provide angular orientation information and the ring data should yield scale information on the input object. A new optical system that can compute the moments of an input image is also considered, since such features are well-known to be attractive geometrical image features. Stereo correlations (used in topographic map synthesis) also appear appropriate for this application. The shape of the autocorrelation peak of the deformed object can contain significant information that may be of use if the effects of distortions on the peak intensity of the correlation pattern are too severe. Image preprocessing (edge enhancement, etc.) will be considered to help maintain correlation in different applications and to enhance the performance of pattern recognition correlators. Image encoding refers to the use of specific patterns rather than simple circular or rectangular shapes. Image segmentation refers to the location and calculation of the deformations for several (e.g. 50) regions of the model, rather than a continuous deformation description. This is the approach we will use and emphasize. The estimator noted in Table 1.1 is used

to determine the deformations of the object from a given set of measured features.

Most of our approaches will involve the measurement of the deformations of separate regions of the object. If 100 such regions must be investigated, then we must extract features from each of these regions or perform 100 auto-correlations. The amplitude of the vibrations in the wind tunnel will affect the measurement accuracy and the rate at which the various measurements must be obtained. If the vibration amplitude is small and the model deformation is in steady state, then it may be possible to sequentially perform the 100 measurements. Otherwise (and this appears preferable), all 100 measurements must be obtained in parallel and real-time to ensure that the relative positions of each of the separate regions of the object are measured at the same instance of time (and hence are independent of vibrations). The high computational rates required to achieve this make the use of advanced high-speed and parallel-processing techniques, such as optical data processing, appear most attractive.

Following initial tests on samples of the model (Section 1.2), we determined that the model surface was sufficiently diffuse to allow patterns to be imaged onto it. This therefore allowed the use of many more techniques. We modified many of the techniques in Table 1.1 to include the projection of various patterns onto the object. We also expanded our initial list of candidate techniques to include the items noted in Table 1.2. These represent classic deformation measurement techniques, with the addition of fringe multiplication and phase conjugation. Fringe multiplication was included to improve the sensitivity of the conventional projection moire methods. Phase conjugation

techniques were included as one approach to overcome the turbulence and index of refraction changes in the imaging medium. These topics and several initial tests performed using these methods were included to quantify the performance possible and to uncover unforeseen difficulties in such methods.

TABLE 1.1 Initial New Coherent Optical Techniques Considered

Fourier Transform Coefficients	Correlation-Shape Analysis
WRD Fourier Transform Features	Preprocessing
Space-Variant Transformations	Image Encoding
Moments	Image Segmentation
Stereo-Correlations	Estimator

TABLE 1.2 Additional Coherent Optical Techniques Considered

Holographic Interferometry	Projection Moire
Contour Holography	Speckle
Shadow Moire	Phase Conjugation

1.2 WIND TUNNEL MODEL SAMPLE TESTS

A sample of the typical material used in tests in the wind tunnel was obtained from NASA Langley. It contained three regions of material (characterized by different finishes) and hence each region of the material exhibited different optical properties. The long (right-hand end) of this test sample

is the most specular region (it has a very small reflection acceptance angle tolerance). The mid-region of this sample is the most diffuse (Lambertian) region and the short (left) end of this sample is the least diffuse region. The right end of this sample could not be easily photographed, since the camera was constantly "blinded" by the strong reflectance from this material when it was oriented near its reflectance angle. At other angles of observation and incidence, no light was reflected. Our initial concern in testing and analyzing this sample was to determine if a pattern could be projected onto the target object and photographed. All of the photos that follow in this section were obtained on high-contrast film (since a binary pattern was projected onto this target sample). We considered the use of white light imaging of a grating onto the object (using a 300W projector bulb, imaged through an aperture onto the grating and then with an imaging lens onto the sample, with the optical axis normal to the surface of the material) and with the use of a 633nm laser (collimated, illuminating a pinhole, and through it the grating pattern imaged normally onto the sample).

Figure 1.1 shows the results obtained. The left column shows the images obtained with white light illumination, and the right-hand column shows the images obtained with coherent laser light. The bottom figure shows the entire sample. As seen, good quality images were obtained for the left (short) end of the sample at most angles of illumination. This is a good diffuse Lambertian surface. The long end of the sample was found to be too specular and gave poor images in all cases. The photographs shown are insensitive to exposure because of the high-contrast film used to obtain these images. From these initial sample tests, we conclude that a non-contact optical approach in which a pattern

is imaged onto the surface is applicable (thus, associated holographic interferometry and Moire techniques are also suddenly appropriate) since a model surface such as the middle or left end can be expected.

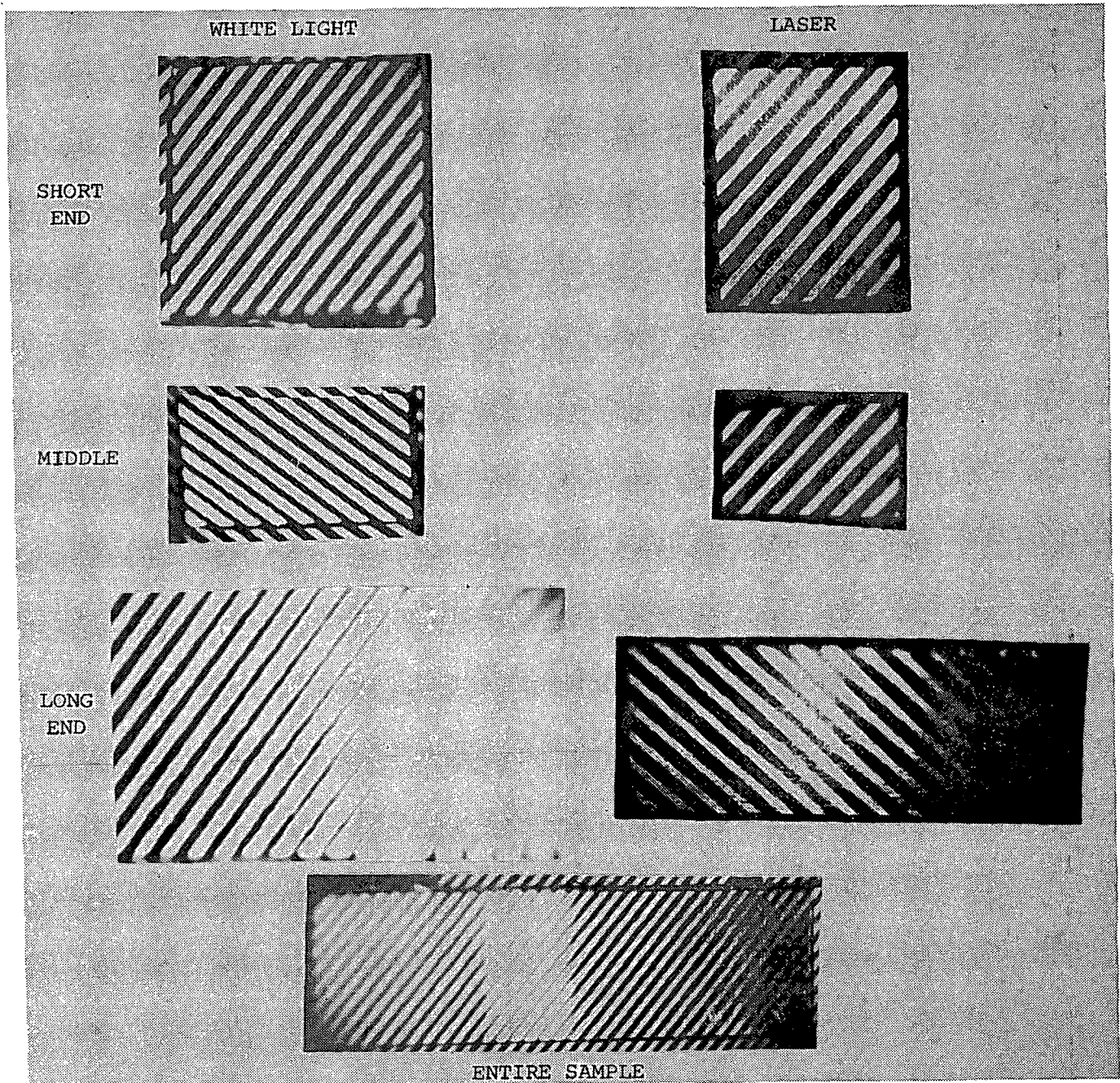


FIGURE 1.1

Photographs of Sample Using White Light Source and
Using Laser Source

1.3 SCOPE OF REPORT

The major emphasis of this one year research study was to provide an initial survey of the ten techniques noted in Table 1.1 (and six other techniques, such as those noted in Table 1.2, which arose in the course of this research) with primary attention to their application to the NTF problem. Applications to other distortion measurement problems at NASA was a secondary goal. The objective of this study was to determine if conventional Fourier transform, correlation and other similar coherent optical data processing techniques and systems were appropriate for the NTF (or other) NASA data processing applications. In all cases, attention was first given to the accuracy obtainable with the different methods and to the system components required to achieve the needed accuracy. Pursuing sixteen different approaches in one year with two people obviously means that only preliminary results can be expected and that emphasis should be given to determining which techniques (if any) are appropriate and merit detailed further study.

Our general remarks and conclusions on several of the items noted in Table 1.1 are now addressed, since they affect the decisions we made in the course of our studies of the other techniques. We determined that image preprocessing was not a vital operation. Thus, it was not pursued in detail. Image segmentation was felt to be vital and necessary (i.e. recording deformation data on 50-100 separate target regions). It was thus used throughout, except for our new modified moire technique we discuss in Chapter 2. It appears to be possible to extract the necessary target deformation information on the full object by extrapolation and interpolation from the deformations in 50 specific regions of the target. We assume that the target deformations are uniform within each of these

50-100 local target regions. Image encoding was likewise felt to be essential to allow the necessary accuracy to be obtained. Our results in Section 1.2 showed that images projected onto the model could be subsequently reimaged. Thus, in all cases, we will consider projection (or only where necessary, printing) of a pattern (such as a grating, PRN code, etc.) onto 50-100 separate regions of the target model. This is preferable to the use of simpler circular or square objects, because the higher space bandwidth product of the pattern provides much more change with deformation and much more processing gain in the system.

In Chapter 2, we discuss the holographic technique (Table 1.2), the methods we selected to pursue (particular emphasis was given to projection moire and fringe multiplication techniques), our laboratory experiments performed on these approaches, our new results and our conclusions and recommendations. In Chapter 3, we briefly note the results of our space-variant transformation, stereo correlation, phase conjugation, and correlation shape studies. Major attention in our research was given to feature extraction techniques, especially the Fourier transforms and moments. Our work in this area is summarized in Chapter 4. Our summary and conclusions then follow in Chapter 5.

2. INTERFEROMETRIC, MOIRE AND SPECKLE TECHNIQUES

2.1 INTRODUCTION

Following our tests on the wind tunnel model (Section 1.2), we included the techniques noted in Table 1.2 and other variations of them in our research. Much of our work on these approaches concerned the study of the many possible techniques of this type and assessing their applicability to the NTF problem. [1] is quite useful in this regard. We thus do not include reference to other individual papers that describe each technique. Our initial assessment and a brief discussion of the various methods we considered is included in Section 2.2. Our primary concern was to isolate the major problems and issues to be addressed for each approach and by brief initial laboratory tests, determine and verify the most promising techniques and uncover any unforeseen problems. Our initial experimental data and results are presented in Section 2.3. They include the use of projection moire, our demonstration of the increased accuracy possible with fringe multiplication, and other new methods to use such techniques for the NTF wind tunnel measurement problem. In Section 2.4, we summarize our results and suggest several new techniques to employ this method and to enhance its use even further.

2.2 OVERVIEW

In Table 2.1, we summarize the techniques we considered and our remarks on each. Holographic interferometry is sufficiently accurate. However, it is too precise. Specifically, too many fringes are produced and the analysis of the output fringe pattern (as well as its detection and the sampling of it) is very complicated. Hence, this approach is rejected. Contour holography involves making two exposures of the object pattern with two wavelengths of light, superimposing

TABLE 2.1 Interferometric and Other Techniques Considered

TECHNIQUES	REMARKS
Holographic Interferometry:	Too many fringes. Hard to analyze output results.
Contour Holography (2 Wavelengths):	Appears attractive. Requires pulsed laser with 2 wavelengths.
Scanning Heterodyne Interferometry:	Scan 2 beams at 2 wavelengths and interfere. Maintaining superposition of beams is a problem.
Speckle:	Ensuring overlap of speckles limits measureable deformation displacement.
Shadow Moire:	Requires grating close to the object, poor sensitivity, insufficient accuracy.
Reflection Moire:	Not practical for vibrating deformed objects.
Contact Moire:	Requires pattern on target.
Differential Moire:	Superposition of deformed and undeformed patterns.
Holographic Moire:	Requires 2 exposure hologram and high stability requirement.
Projection Moire:	Preferred technique, needs increased accuracy by fringe multiplication.

the patterns and analyzing the results. This is a good, sound and appropriate approach. It is useful of course only for calculations of out-of-plane displacements. It provides better sensitivity for a given pattern than does conventional moire. However, since we do not have the required multiple wavelength lasers nor pulsed lasers, we did not pursue it further with laboratory tests.

Scanning heterodyne interferometry employs the scanning of two beams at two different wavelengths across a pattern, interfering both and detecting the phase of the beat frequency provides the resultant information. The major problem with this technique is the requirement to keep the two beams superimposed during scanning. Fabrication of the necessary system to achieve this is a quite extensive effort and it cannot be done casually or the performance obtained will suffer. A new idea and technique that one could pursue is to use two coded signals, correlate them and obtain the phase and hence the range shifts from the phase of the correlation output. Speckle techniques were also considered. Initially, they appeared to be quite attractive. However, when quantified, we found that the maximum target displacement possible for which overlap of the speckles could be insured was only 1.5mm. This is significantly worse than the displacements required in the NTF problem and application. Thus, we did not consider this technique further.

Various other techniques [2-4] were also considered that appear more promising for the specific wind tunnel testing program. These included shadow moire methods [4]. In these techniques, a grating is placed close to the test surface and illuminated with a point source. The shadow of the grating is then placed onto the object. When an image of the shadow is viewed through the grating, a moire contour results. The grating must be placed close to the object to keep the shadow in focus over the depth of field. As a result, the sensitivity

achievable with this technique is quite poor. Only 1mm deformation resolution is possible. Thus, for this specific NASA application, this technique is not viewed as practical since its accuracy is insufficient.

Reflection moire was also considered. It is similar to the shadow moire technique, except it is appropriate for specular rather than diffuse surfaces. In this scheme, a reflection grating is imaged off from the object and passed through a reference grating. In this system, it is necessary to view the object at the specular angle. This is not practical for NTF objects with the deformations and vibrations expected. Deformations and vibrations will determine where the image projects to. For these reasons we do not consider this technique further.

Contact moire techniques were also considered. In this scheme, a grating is placed on the object and an image of it, after deformation, is compared to a reference grating. This technique is easier than the previous one since one only needs one access angle to implement it. The major objection to this technique is that again one must contact the grating to the model and this may disturb the model. In contact moire, the fringes depend upon the displacement between the input plane and the output plane. Thus, such methods can provide strain measurements; this is not always desirable and the analysis of the resultant pattern that is produced with such techniques is more complex than with other moire methods.

Differential moire is yet another concept we considered. In this technique, a photograph of the grating on the undeformed object itself is used as the reference. In this case, the object's topography is not present in the resultant moire pattern, rather only its distortion are, hence the name differential moire. It is also possible to project a second grating onto the object and to produce the moire on the object itself. If the projected grating is a photograph of the grating on the deformed object, then the topography of

the object can again be removed. In the indicated NASA application, the topography of the object is probably desirable, thus this technique does not appear to merit further attention.

In the holographic moire technique that we considered, one makes a realtime double exposure hologram of the test object and the reference object and one compares the holographic fringes between the two. This technique is very sensitive, however vibration problems and high stability are required in the processor and the fringe pattern that is produced is quite difficult to easily interpret. For these reasons, it does not appear to be attractive and practical. The final

The final technique considered is referred to as projection moire [3]. This is a superior technique to the aforementioned ones. In this method, a grating is projected onto the test object. It is then photographed at an angle not equal to the projection angle and the image that results is compared to the image of the reference grating to produce the desired moire. If the reference grating is an image of the grating on the object and if this is projected through an image of the distorted object, then the contour of the object can again be removed and the moire fringes will show only displacements of the object from the reference positions. This will occur for all object regions. This appears very appropriate for the wind tunnel application.

The sensitivity of moire techniques is

$$\Delta z = \frac{p}{\tan\alpha + \tan\beta} ,$$

where p is the period of the grating, and α and β are the angles of projection and viewing with respect to the normal to the object. As the surface shape changes, so do the angles and hence so does the fringe pattern. From an analysis of the fringe pattern, the shape (i.e. the deformation) of the object can be obtained.

As the technique we decided to experimentally test and evaluate, we chose projection moire for the reasons noted above. It is the most attractive and appropriate one. It can potentially provide analysis of deformations for the entire object using only one image and without the need to print a pattern onto the model. This technique provides only out-of-plane deformation information, of course. To increase the deformation measurement accuracy obtainable from this technique, we suggest the use of fringe multiplication by optical processing. The idea in this technique is to increase the frequency of the reference and deformed gratings, then to superimpose the two. This increases the number of fringes and hence the deformation measurement accuracy possible. This technique is very attractive since it allows us to use a lower frequency grating and thus more moderate quality optics. With fringe multiplication, we can then achieve the same accuracy as one could obtain using a higher frequency grating and more expensive optics.

A second new approach that we suggest is the formation of a projection moire pattern of the entire object (at low resolution) and then to form an analysis (by fringe multiplication using optical processing techniques) of different portions of it. This will allow us to measure displacements in certain areas to high accuracy and yet obtain the full-field image with less accuracy and with less complex fringe pattern required. This can easily be achieved by aperturing off regions of the moire pattern of the entire object and applying fringe multiplication only to these regions. We can also use optical data processing to enhance low-fringe contrast (due to blur, lens aberrations, etc.). This can be achieved by spatial filtering the output dc order in the Fourier transform plane and thus removing the background. We can also remove high frequency noise (dust

etc.) by use of a donut-shaped spatial filter in the Fourier transform plane. This will greatly enhance the contrast and quality of the moire image produced.

2.3 PROJECTION MOIRE AND FRINGE MULTIPLICATION

To become acquainted with the various techniques for surface measurements and to uncover unforeseen problems, various projection moire patterns were obtained. Several examples of these data follow. The object chosen was a gas canister cylinder with an indentation on one side. Data was obtained with both white light and coherent laser illumination. The white light source data was the easiest to observe and thus data obtained with this system is included. The optical system used is shown in Figure 2.1. The projection arm of the system consists of imaging optics that project an image of a grating pattern (grating 1 = G_1) onto the object. The observation arm of the system consists of imaging optics that project the image of the grating pattern as it appears on the object onto a camera through a second grating pattern (grating 2 = G_2). The superposition of the G_2 pattern and the image of G_1 on the target is then observed by eye or through a camera and monitor. For our experiments, identical optics were used in both arms of the system. Thus, the optical axes in both arms are equivalently in the same plane and the lines in both gratings are perpendicular to the above plane. We chose to use $d_1 = d_1' = 251\text{mm}$, $d_2 = d_2' = 1255\text{mm}$ and imaging lenses with $f_L = 209\text{mm}$. This yielded a magnification $M = 5$ for the projection arm. The gratings G_1 and G_2 were identical with a spatial frequency $u_G = 100$ lines/inch = 4 lines/mm.

We could visually observe the grating output on the object with our eyes d mm behind G_2 . However, due to our light budget, photographs of the contour

ORIGINAL PAGE IS
OF POOR QUALITY

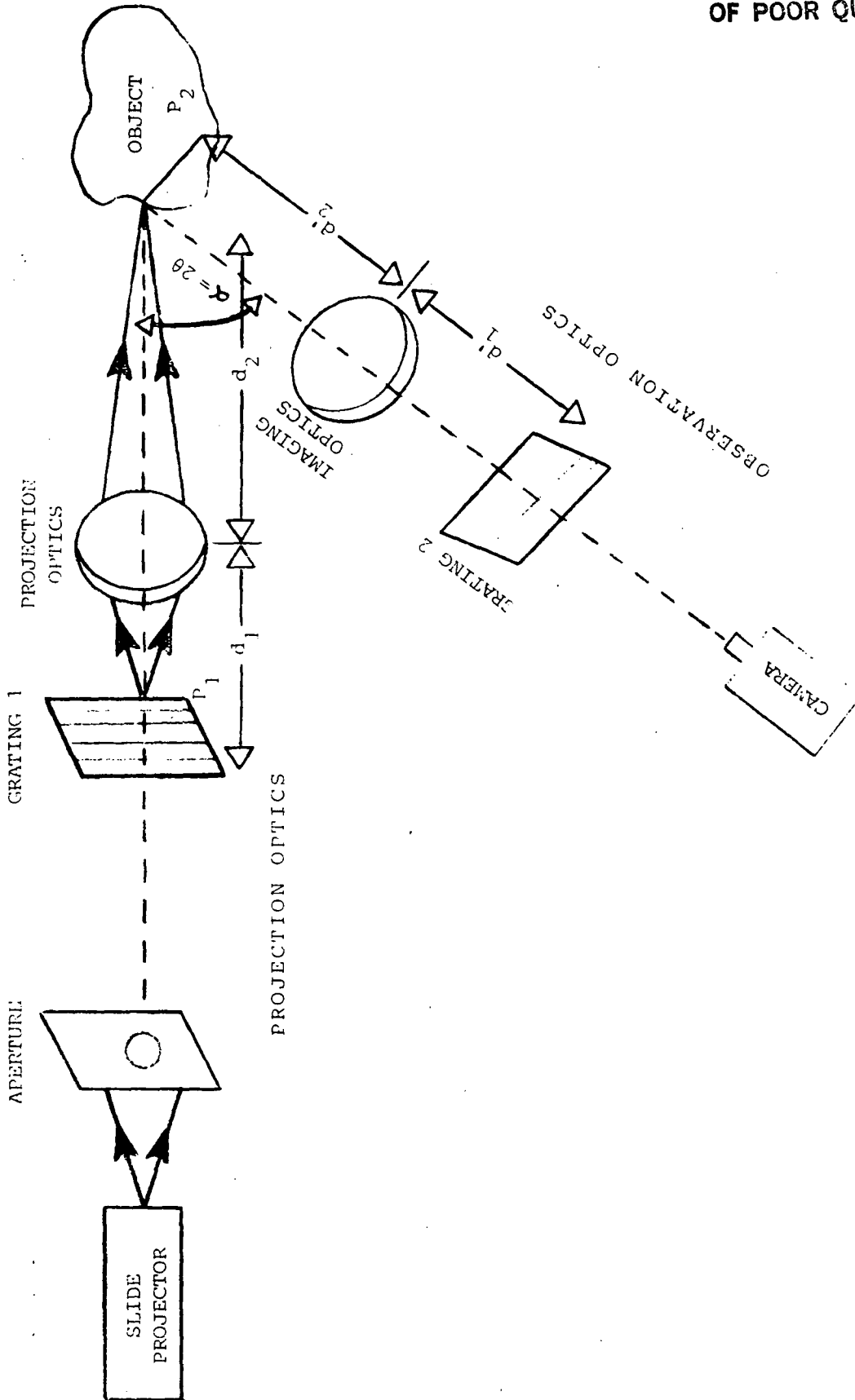


FIGURE 2.1
Optical Setup for projection Moire Surface Metrology Tests

fringes produced were not of good quality. Thus, we chose to simply focus the camera in the observation arm of the system directly onto the object and to photograph the projection grating pattern obtained (this is the image of the grating as projected onto the object). We then place this photograph in contact with G_1 in plane P_1 of the projection system, we remove the object, place an observation screen in place of the object, and photographed the resultant moire contour pattern obtained on this screen at plane P_2 of Figure 2.1. In Figure 2.2, we show an image of G_1 projected onto the object. In Figure 2.3, we show the projected moire contour fringe pattern observed. The contour lines or the equal-order surfaces in the moire pattern are perpendicular to the bisector of the angle $\alpha = 2\theta$ between the projection and observation arms in Figure 2.1. Thus, the distance between the two equal-order surfaces (i.e., adjacent contour lines in Figure 2.3) is

$$d_0 = \frac{p'}{2\text{Sin}\theta} , \quad (2.1)$$

where p' is the pitch of the projected grating and $2\theta = \alpha$ is the angle between the projection and observation arms.

For our experiments, the pitch of the original grating G_1 is $p = 1/u_G = 0.25\text{mm}$, the magnification $M = 5$ and thus

$$p' = pM = M/u_G = 5/4 = 1.25\text{mm}. \quad (2.2)$$

For our system, $\text{Sin}\theta = 0.125$ and thus

$$d_0 = p'/2\text{Sin}\theta = 1.25/2(0.125) = 6\text{mm}. \quad (2.3)$$

Thus, in our laboratory system, the spacing between the contour fringe lines,

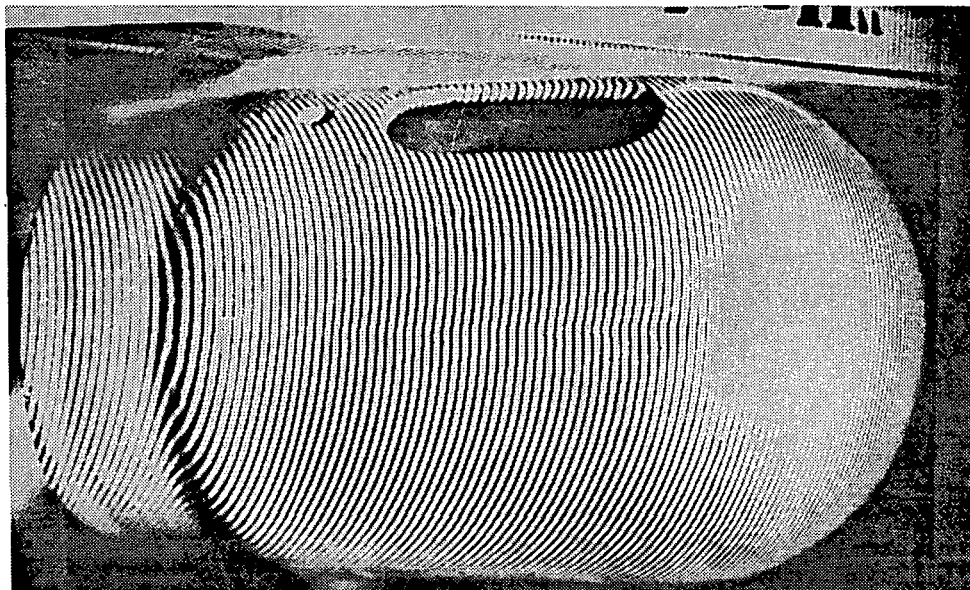


FIGURE 2.2
Image of Original Grating Pattern on Object

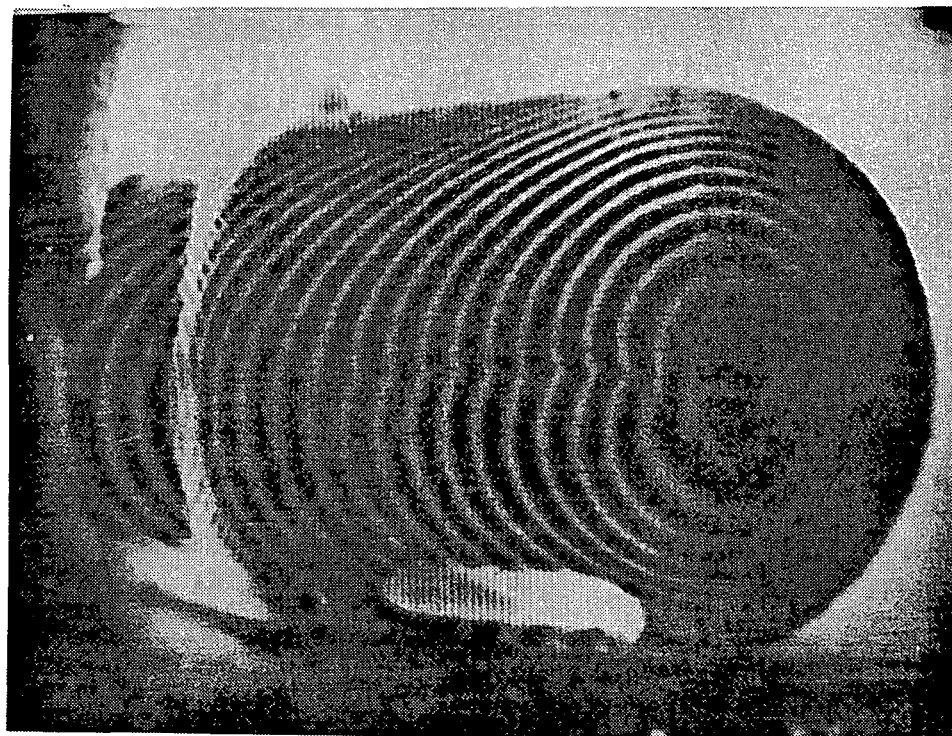


FIGURE 2.3
Moiré Image (Object Contour More Apparent)

in the moire pattern in Figure 2.3 corresponds to displacements of the object's surface of $d_0 = 6\text{mm}$. If a grating with $u_G = 20$ lines/mm were used, the distortion between consecutive equal-order surfaces would correspond to 1.25mm depth differences in the object. Thus, from our experiments, we found that moire contour patterns are easily produced and obtained with white light illumination.

It should be noted that telecentric or collimated imaging light is very helpful in moire pattern analysis, since it greatly simplifies the mathematical description of the results obtained and the associated analysis of the resultant fringe pattern obtained. Specifically, the corresponding object displacements associated with different contour fringes will be a constant in this case. We also note that projection moire allows out-of-plane deformation measurements to be obtained. In projection moire, obtaining an adequate depth of field is an issue of concern. Thus, large pitch gratings are attractive for use, since less depth of field problems then result. When the grating pattern is imaged onto the full object, the depth of field requirements become even more demanding. Thus, an accuracy of 1mm in the displacements of points on the object is realistically possible with projection moire techniques. This will prove to be adequate for our NTF application as we will see below.

To improve the object measurement accuracy beyond 1mm to the $64\mu\text{m}$ resolution required in the NTF problem, we suggest the use of fringe multiplication [10]. In this technique, the deformed grating pattern observed on the object (or the associated contour fringe pattern) is multiplied by a different grating (G_3) with a different pitch from that of the original grating ($G_1 = G_2$). The Fourier transform of this product of two grating patterns is formed. The N-th order in the Fourier transform of this composite multiplicative grating pattern will

have N fringes for each original image fringe. Thus, this technique allows the fringe accuracy, and hence the accuracy associated with adjacent contour fringes, to be increased by a factor of N .

If we assume that we have an original fringe accuracy of $F = 1\text{mm}$ and that we can read fringe patterns to an accuracy of $A = 0.25$ of a fringe, then fringe multiplication by a factor $M_F = 10$ provides an accuracy in the target deformations of

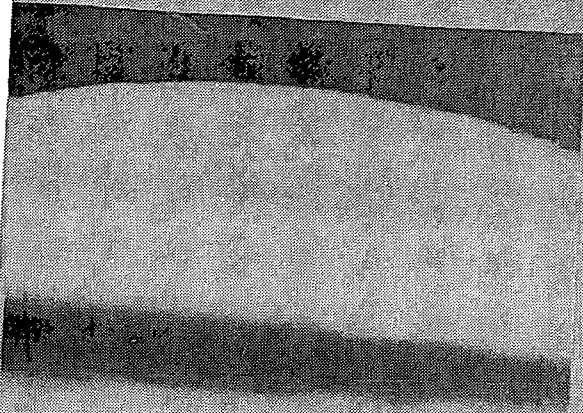
$$F' = F \cdot A / M_F = 1(0.25) / 10 = 25\mu\text{m}, \quad (2.4)$$

which is better than the accuracy required in the NTF problem. Thus, this technique of projection moire, augmented with fringe multiplication, appears most promising and attractive and capable of providing sufficient accuracy needed in the NTF application.

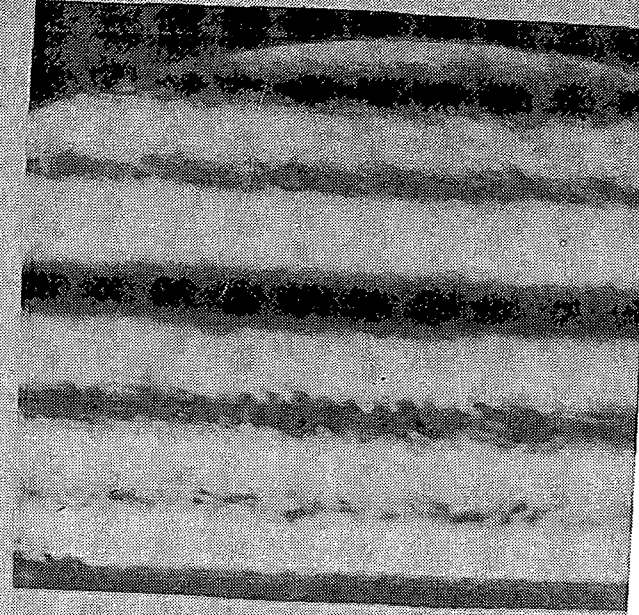
To verify the accuracy improvement possible in projection moire using fringe multiplication, a simple experiment was conducted. The original moire contour pattern was placed in contact with a grating of slightly different frequency and the Fourier transform of the product inputs $f_1 f_2$ was formed. This yielded the output pattern

$$\mathcal{F}[f_1 f_2] = F_1 * F_2, \quad (2.5)$$

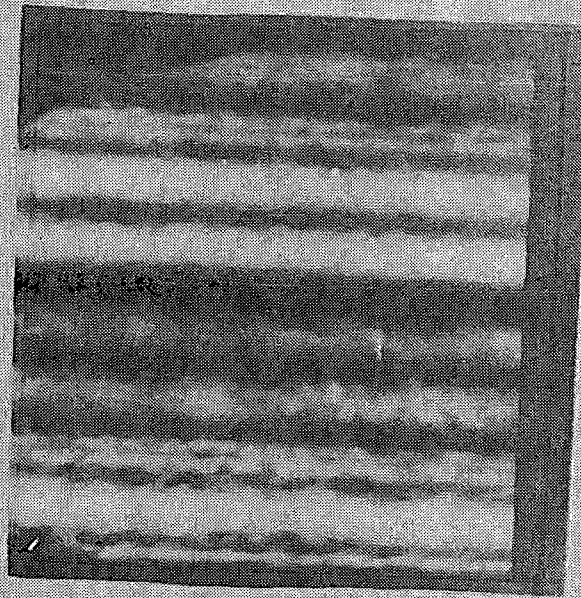
where F_1 and F_2 denote the Fourier transforms of f_1 and f_2 . It is possible to obtain moire fringe multiplication by using two gratings of different pitches, or with two gratings of the same pitch (if one grating is rotated with respect to the other). In Figure 2.4, we show two of the fringes in the original moire pattern and their multiplication by factors of 2 and 4 using the aforementioned fringe multiplication technique.



Original Pattern



Multiplication by 2



Multiplication by 4

FIGURE 2.4
Examples of Fringe Multiplication for Improved Accuracy Projection Moire Contouring.

2.4 ADVANCED APPROACHES AND SUMMARY

As described in Section 2.2 and as quantified by our initial experiments in Section 2.3, projection moire (when augmented with fringe multiplication) can provide the necessary accuracy and performance for the NTF problem. The depth of field requirements for the projection of the original grating pattern were noted. Application of projection moire requires that different points on the object be treated separately (as we have done), since this significantly reduces the depth of field requirements for the projection optics.

We now note several advanced techniques to further enhance the performance and implementation of such an NTF processor.

- (1) We note that the resultant moire pattern is a combination of image shape and image deformation information. We suggest (for future work) that one can separate these two effects by use of differential moire techniques (i.e. by forming two moire patterns, one with distortions present and one without distortions present). This would provide an output display with only the required and desired target deformation information present on it, rather than the shape of the object also included.
- (2) We note that it is also possible to contact-print the grating pattern directly onto the object. If this is done, then in-plane target deformations can also be obtained by this technique (in addition to out-of-plane distortion information).
- (3) The evaluation of the optically-generated moire contour patterns can still require extensive post-processing. The use of optical Fourier transform and convolution techniques that can aid in

such an analysis of the fringe pattern contour and deformation information present.

- (4) Optical matrix-vector techniques [11] appear most appropriate to relate deformations at different spatial locations to global deformations (in-plane and out-of-plane distortions) appear possible.

As noted earlier, all of these moire techniques require a non-specular surface. The actual model surface is between the extremes of specular and diffuse. Thus, a range of angles exist over which images with high contrast can be obtained from images projected onto the model. Vibrations are of concern in all systems. The moire technique in which the entire model is imaged at once is thus most attractive, since any sequential analysis technique will be plagued with practical problems associated with having deformations of different points of the object at different points in time (i.e. at different points in a vibration cycle). If the vibrations of the target are periodic, we can probably sequentially image and avoid such difficulties.

Our proposed techniques are new, in the sense that they have seen only limited application and in no instance has the accuracy required in the NTF problem been considered using this method. Hence, fringe multiplication appears most attractive for the NTF applications. The output detector system to analyze the moire pattern produced still remains to be addressed.

3. CORRELATION AND OTHER TECHNIQUES

3.1 INTRODUCTION

In this chapter, we consider various alternate approaches to the wind tunnel test and measurement problem that received only initial consideration and analysis during our study. These include the effects of turbulence and vibrations, the use of phase conjugate optics to remove these effects, the use of time-average moire and real-time moire and how they affect this problem, plus the use of pulsed and video moire. Finally, we consider stereo-correlation methods to some extent and finally a novel autocorrelation shape analysis concept. We then briefly address space-variant transform methods and techniques for deformation analysis. Our summary and conclusions are then advanced.

3.2 TURBULENCE AND VIBRATIONS

Initial studies indicate that various turbulence, shock waves, and other such effects which result in changes in the index of refraction of the imaging medium will be present in the wind tunnel data. We have considered several approaches to overcome this problem. Only brief remarks are advanced on each.

The use of phase conjugate optics was considered. This technique is useful in imaging through a turbulent media. However, we have been unable to devise a way to apply it to the NTF problem, since the turbulent medium lies between us and the object. Any architectures we devised and studied removed the effects of the turbulence as well as any deformation effects on the model itself.

The use of time-average moire [5] was also considered. In this approach, we simply time-averaged the moire for a vibrating object over a time long with respect to the frequency of the vibration. The vibration frequencies in the NTF system are noted to be

up to 200Hz. The result of such a time-average is that the only points in the grating image that will be seen are those at the two extremes of the vibration cycle. All intermediate ones average out, since they are random. In this manner, the moire that results is due to grating images at the two extremes of the deflection and thus maximum object deflection is measured. The use of different integration times can allow different vibrations to be addressed. However, the vibrations must be well-behaved. Further analysis is necessary and details are necessary to determine if this is the case in the NTF system.

Real-time moire is another possible candidate approach we considered. This technique can provide the time-history of the dynamic vibrations for the entire object. However, vibrations can also occur due to the tunnel, air turbulence, acoustic noise and even the mechanical support for the processor. In real-time moire, considerable vibration isolation is necessary and multiple vibration effects will be present in the data. Thus, any such approach is expected to require quite significant analysis to extract out the separate vibration effects included. Other techniques considered include pulsed moire. In this concept, two short pulsed images of gratings at two different times are produced. The moire from the overlap of these patterns then maps changes in the topography of the model, rather than displacements between two time pulses. Thus, this technique does not appear appropriate.

Video moire [6] is another technique that may be worth pursuing. We did not evaluate its possible potential

3.3 SPACE-VARIANT IMAGE PROCESSING

An alternate technique that we briefly considered was the use of various space-variant optical processing concepts. This class of processor is much more flexible and powerful than the conventional shift-invariant systems. These systems comprise a coordinate transformation preprocessing step followed by a

Fourier transform, correlation or similar shift-invariant operation. The resultant system architecture (and its impulse response) are space-invariant. The attractiveness of such techniques to the present wind tunnel deformation measurement problem are that by proper choice of the coordinate transformation, one can obtain an output correlation peak (whose intensity is invariant to various geometrical distortions in the input pattern) whose location is proportional to specific deformation parameters in the input pattern. From the correlation peak location, object deformations can be extracted and thus data obtained on the distortion parameters of the object pattern.

One specific example of this concept is the optical Mellin transform [7]. In this solution, a logarithmic transformation is applied to the input data and this is followed by a Fourier transform. The result is a Mellin transform of the input image. Mellin transforms are most attractive for scale-invariant processing, since the amplitude of the Mellin transform coefficients are invariant to scale changes in the input object. Scale changes in the object appear as phase terms in the Mellin transform pattern. Thus, to extract scale (or associated out-of-plane rotations which can be modeled as different 1-D scale changes), we must extract the phase of the Mellin transform coefficients. One can extract such information by heterodyne detection, however the resultant system will become quite complex.

A simpler, and often times preferable, solution is to perform a correlation using Mellin transforms rather than Fourier transforms. In this instance, the classic frequency-plane optical correlator [8] can be used. The correlation is simply performed between coordinate-transformed patterns rather than the conventional Euclidean space versions of these patterns. In this case, the amplitude of the output correlation peak will be invariant to scale changes in the input object and the position of the correlation peak will now be

proportional to the scale changes between the reference and input object. Such methods of extracting phase information are preferable.

If we can insure that each object pattern is positioned approximately in the center of the input plane, then such techniques are appropriate (they are space-variant, thus they are not shift-invariant, and hence we require the input object to be centered in the input plane). By performing a gross correlation of the entire object, it appears that such centering can be achieved. The accuracy associated with this technique should be quite high, since now we position-encode the associated scale change data. The shortcomings of this system are the requirement to perform many correlations, with the additional requirement of a coordinate-transformation preprocessing step. Such systems and architectures are of course possible, however we again choose not to consider them for future detailed study at this time. Instead, we defer to simpler systems (see Chapter 4).

3.4 STEREO CORRELATION TECHNIQUES

Stereo correlation [9] involves comparing the correlation pattern obtained from a stereo pair of photographs of an object taken prior to deformation with the correlation pattern obtained from a stereo pair of photographs taken after deformation (only out-of-plane deformations are appropriate). The relative locations of the correlation peaks in one correlation pattern, with respect to the locations of the same peaks in the other pattern provide information about the out-of-plane deformation of the object. By comparing N points in the undistorted object to the corresponding N points in the distorted object image, we can produce an n -th order polynomial approximation for the object's distortion.

From photographs of an object obtained from two different viewpoints (this is easily possible with the viewing port arrangement present in the wind tunnel), it is possible to obtain a full description of the object in terms of contours and profiles by using this stereo correlation technique. This procedure is used extensively in topographic map plotting. In the course of our work, we have expanded this technique and applied it to the measurement of out-of-plane deformations in wind tunnel imagery. Since in-plane translational deformations can be accommodated without the need for stereo photographs (by using only one pair of photographs), in-plane deformations will be discussed only briefly. In Figure 3.1, we show a simple system for forming a stereo pair of photographs. In the ideal case of vertical photographs, the camera axes are parallel to each other and normal to the reference plane and both image planes are perpendicularly centered on the plane $y = y_0$.

In Figure 3.1, f is the distance between the camera lens and the image plane. The height of the object is h . It is defined with respect to the reference plane. The separation between the camera axes is defined as the stereo base B . The differential x -parallax is

$$P_x = x_1 - x_2 = fB/(H - h). \quad (3.1)$$

By simple geometry, one can derive (3.1). From (3.1), we see that as the height of the object h varies from point-to-point in the image, the distance $x_1 - x_2$ between the image of the point in the two image planes also changes. For the case in which the image planes are centered at $y = y_0$, the differential y -parallax will be zero.

ORIGINAL PAGE IS
OF POOR QUALITY

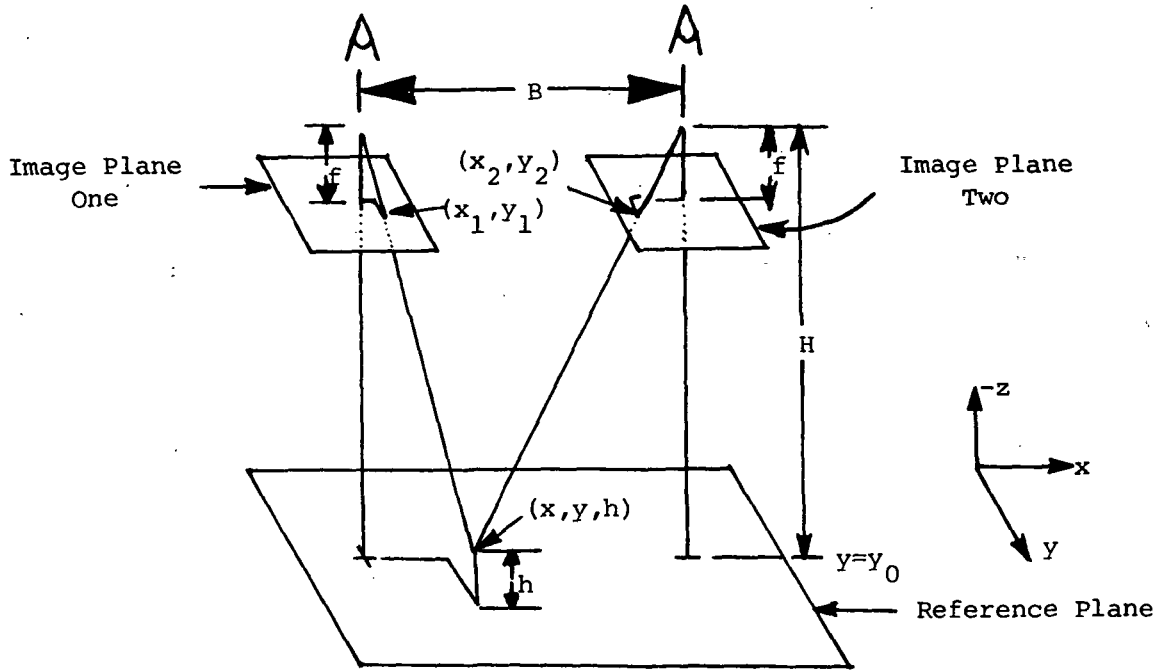


FIGURE 3.1 Schematic diagram of a system that can produce stereo-pairs of photographs.

We now discuss how to relate object deformations to the locations of points in the two image planes. We consider a pattern to be placed at coordinates (x, y) on the object. The image of this pattern will then be located at some coordinates (x_1, y_1) in image plane 1 and at coordinates (x_2, y_2) on image plane 2. If the difference $x_2 - x_1$ is determined, then the height of the object at the point (x, y) can also be determined from (3.1). For the wind tunnel problem, this would be done for selected points on the model. These data can then be used to provide a contour map of the height or deformations of the target. This is not the

goal in the wind tunnel problem however. In our case, we desire the object's deformation. A suggested procedure to achieve this is discussed in the next paragraph. The cross-correlation operations required in this processing lend themselves quite nicely to optical processors which can thus determine the relative position of each pattern in the two image planes. If different patterns with minimum cross-correlations (e.g., Walsh-Hadamard matrices) are used, cross-correlations between separate patterns will be minimized and thus the required correlations can be performed from one view of the target (if sufficient resolution is possible for each object pattern).

We now advance a new method to extend these concepts to measuring out-of-plane deformations of an object. The object is assumed to have N patterns on it at N different locations. The number of patterns used, the type of pattern, and their relative positions will determine the accuracy with which the object deformations can be measured. To obtain more detailed and accurate deformation estimations, we can divide the object into more patterns within each segment. Once the object's surface has been prepared as described above, a stereo photograph pair is taken of the N patterns on the object segment. This is done for the undistorted object (before wind tunnel testing). This stereo pair is then used in a correlator to calculate the x-parallax difference for each of the N patterns. This provides us with information on the height of each pattern (in the undeformed object). Next, the object is deformed (i.e., it is placed under wind tunnel testing). A new stereo pair of photographs is then taken of the same N points. This new stereo pair is then used to determine the height of each pattern in the deformed object. The amount of out-of-plane deformation for each point can then be computed by subtracting the height of each pattern object before deformation from the height after deformation.

We note that this technique is useful only for measurement of out-of-plane deformations. If in-plane deformations occur (such as translations), these distortions will not be detectable using the above technique. This can be seen by assuming that the pattern on the object is translated in the object plane by an amount $(\Delta x, \Delta y)$. A corresponding change $(\Delta x_i, \Delta y_i)$ will then result in both image planes. In this case, the parallax difference between the locations in the two image planes

$$(x_1 + \Delta x_i) - (x_2 + \Delta x_i) = x_1 - x_2. \quad (3.2)$$

will be unchanged. We can extend this method to provide in-plane translational measurements by correlating one of the stereo pair photographs taken prior to the deformation with the corresponding photograph taken after the deformation. Thus, with these modifications, both in-plane and out-of-plane distortions can be measured with this technique.

This stereo photometric approach requires the measurement of the difference $x_1 - x_2$ of the locations of a given image point (or object pattern) in the two different stereo views. This can easily be achieved by correlation techniques [especially when the points are actually patterns (which is the case in our wind tunnel application)]. An optical frequency plane correlator (such as the one in Figure 3.2) is thus very attractive for providing such data. We first briefly review the operation of this well-known system [8]. We then detail how this system would be used for our specific cross-correlation stereo-photometric technique for object distortion analysis.

Refer to Figure 3.2. Two images (transparencies 1 and 2), which we wish to correlate are used. To achieve correlation, we will place transparency 2 in the input plane

and a matched spatial filter of transparency 1 in the second plane. The correlation pattern of the two transparencies will then appear in the output plane. The matched spatial filter is formed by placing the pattern in the input plane and interfering its transform and a planewave reference beam. For the case when transparency 1 contains a particular pattern and transparency 2 contains several occurrences of the reference pattern, then the output correlation plane will consist of several peaks of light, with the location of the different peaks of light corresponding to the locations of the reference pattern within input transparency 2.

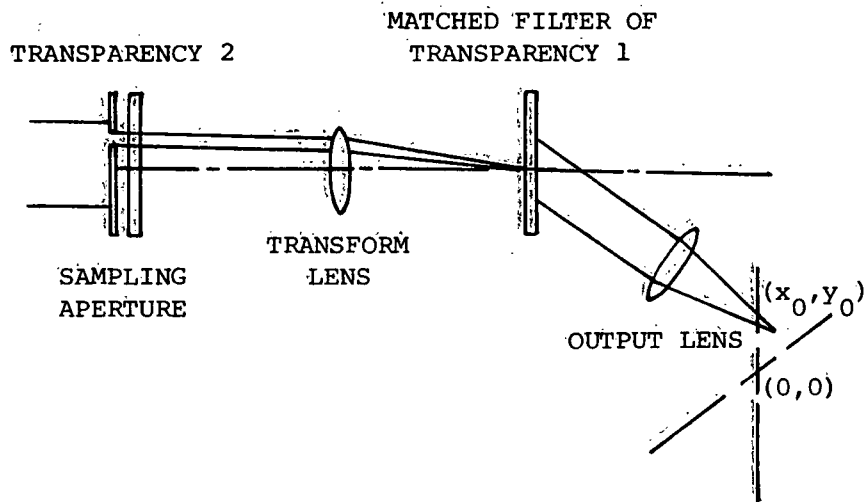


FIGURE 3.2 Schematic diagram of an optical frequency plane correlator.

We now consider the application of this technique to the specific wind tunnel problem. We form two stereo images of the entire target, containing many object patterns. A matched spatial filter of one of these stereo images is placed at the second plane of the system of Figure 3.2. The other stereo image is placed in the input plane of the system. An aperture is moved

sequentially about the input transparency 1. As it moves, separate regions, and hence separate ones of the pattern recorded on the target are illuminated. Thus, in sequence, the output correlation plane pattern will contain peaks of light at locations which indicated the difference $x_1 - x_2$ in the locations of each of the patterns recorded on the target. From these different values, the height of each pattern on the target (undeformed target) can be determined. This procedure is then repeated for the second stereo pair of images (with the target now deformed). By properly combining the outputs from both correlation plane analyses, the deformations of each individual pattern region on the target can be obtained. The moving input plane aperture required can easily be realized with various binary spatial light modulators (without the need for any moving parts) or with available telecentric scanning systems.

The accuracy of our deformation estimations will depend upon the accuracy with which the difference $x_1 - x_2$ (i.e. in our case, the location of the correlation peak) can be determined. Thus, it is quite important to utilize object patterns, rather than points, since the increased space bandwidth product of such patterns will provide much higher correlation peak values and much narrower correlation peaks (thus providing us with a better measure of the desired $x_1 - x_2$ value).

We now consider a specific case and detail the performance of this system. We consider a pattern to be located in the reference plane at coordinates (x, y, z_1) . From the correlation of a stereo pair of photographs of this pattern, the location $x_1 - x_2$ of the correlation peak can be obtained and from it the x-parallax difference. We consider the case when the focal lengths of the two Fourier transform lenses in Figure 3.2 are equal. For this case, the height of the pattern on the undistorted object is given by

$$z_1 = H - [(fB)/(x_1 - x_2)] . \quad (3.3)$$

Next, the object is deformed. A new stereo pair of images of it is produced and these are also correlated. For this case, we assume that the deformed object is now located at coordinates (x, y, z_2) . From the correlation output of this second (deformed) stereo pair we obtain a correlation peak at $x'_1 - x'_2$. The height of the pattern on this deformed object is then found to be

$$z_2 = H - [(FB)/(x'_1 - x'_2)] \quad (3.4)$$

The out-of-plane deformation of the particular object is then found by combining (3.3) and (3.4) to be

$$z_2 - z_1 = fB\{[1/(x'_1 - x'_2)] - [1/(x_1 - x_2)]\} = \Delta z \quad (3.5)$$

If this procedure is repeated for N patterns (located at different positions x_1, x_2 (or in 2-D at y_1, y_2 , etc.)), then an N-th order polynomial can be produced (using the method of least squares, for example) and from this the distortions of the object over its entire viewed area can be obtained to N-th order. The results obtained for smaller regions of each object pattern can also be used and combined to provide information about the deformations across a given object region. In practice, the original set of correlation peak coordinates need only be calculated and stored once. Thereafter, as the input aperture is moved about transparency 2, we obtain on-line the point-by-point height of all patterns recorded on the target.

This technique appears to be quite attractive and appropriate for the wind-tunnel application. The various modifications that we noted in it should be incorporated to provide the best results. In other analyses, we quantified the accuracy obtainable from such a system and found that it appears to be

suitable for the wind tunnel application. Our only motivation for not pursuing this architecture further is its comparative complexity (multiple correlations are required, and a real-time holographic matched spatial filter is needed, together with a real-time input transparency device). Several versions of this system (using photographic film) exist and have been used by Harris Corporation and the Engineering Topographic Laboratory. Thus, although this technique appears to be attractive and useful, we do not consider it further and defer more detailed studies to the simpler architectures and processing systems in Chapter 4.

3.5 AUTOCORRELATION SHAPE ANALYSIS

Another most novel technique which we have suggested, and for which we performed initial experimental tests, is the analysis of the shape of the autocorrelation function for the different object patterns recorded on the target. From this shape analysis, we propose to extract various parameter deformations of the target in each object pattern region. This technique again requires the use of patterns rather than points at various locations on the target. The main motivation for this concept is the fact that the peak value of the correlation will change rather significantly and in addition different distorted patterns can provide the same peak intensity value for the correlation. Thus, separate distortions can give rise to the same peak correlation value I_p . However, the shape of the correlation function has significant information contained in it, besides just its peak value. Specifically, as the pattern becomes distorted, the shape of the correlation function also changes.

We thus suggest that such an analysis of a correlation output pattern can provide the required information on the distortion parameters present in the particular object pattern (or target region) under investigation. Initially,

we considered using cross-correlations between the undistorted object pattern and the distorted patterns present on the target. We found very severe degradations in the peak correlation intensity to occur and feel that these will result in severe detection problems in a practical system. Thus, we then modified our technique to include and require only the computation of the autocorrelation of the distorted object pattern. This is most attractive for many reasons. First, the location of the autocorrelation function in the output plane is known and is fixed (it always occurs in the center of the output plane). Second, the intensity present in this output pattern will remain approximately constant with deformations. This will greatly simplify and enhance detection of this output plane data.

An initial experiment was performed to verify the dependence of the shape of the autocorrelation output on distortions in the input pattern. This was achieved using a scaling optical correlator. An optical matched spatial filter of the original undistorted object was formed and correlated with the original object. A cross-section scan of the output correlation function obtained is shown in Figure 3.3a. Next, the input was subjected to various distortions (i.e. input plane rotations were introduced by simply rotating the input object; scale changes were produced by translating the object along the optical axis. In the scaling correlator used, this introduces scale changes). A new matched spatial filter for the distorted input pattern was obtained, its autocorrelation was formed and cross-sectional scans of it were produced. A cross-sectional scan of a typical autocorrelation for the same object in Figure 3.3a (for a distorted input image) is shown in Figure 3.3b. Comparison of Figures 3.3a and 3.3b shows differences in the widths and distribution of the two autocorrelation functions.

ORIGINAL PAGE IS
OF POOR QUALITY

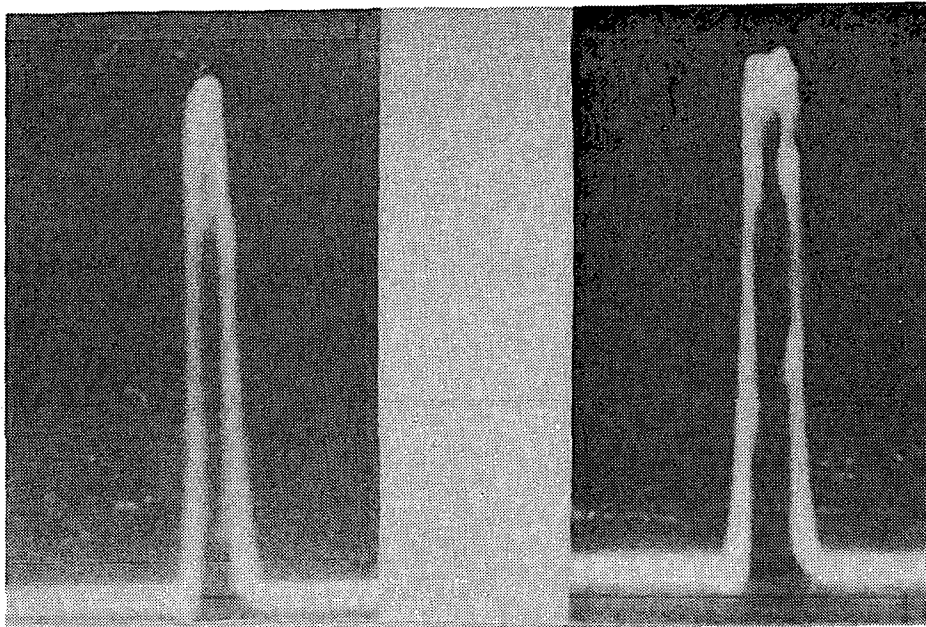


FIGURE 3.3

Cross-Sectional Scans of the Auto-Correlations of an Undistorted
(a) and a Distorted (b) Input Pattern.

Attempts to relate the correlation shape to the input distortions became much more complex than we originally anticipated. Thus, quantitative data was not possible on the accuracy with which input distortion parameters can be measured by this technique. Rather, we elaborate on the various issues involved in such an analysis and note initial results for translations which indicate that sub-pixel distortion parameter measurement accuracy is possible. First, we reiterate that since we perform an autocorrelation, the location of the output pattern is known and fixed. Thus, a small fixed set of detectors can be placed in the output plane. This greatly simplifies the output measurement data. Because an autocorrelation is performed, an optical joint transform correlator appears to be an attractive architecture. However, since the autocorrelation need be evaluated only for several relative shifts of the pattern, it is quite possible to perform the autocorrelation digitally (since evaluation of

the correlation at different shifts involves only a simple projection operation).

Use of an optical correlator introduces several effects which we found to greatly complicate the quantitative interpretation and relation of a sampled autocorrelation function to input object distortions. First, the frequency plane material used in an optical correlator will saturate at dc and low spatial frequencies, thus producing the autocorrelation of an edge-enhanced or high-pass filtered object image. Secondly, the output detectors used to sample the autocorrelation function are area detectors, not point detectors as in a digital correlator. Thus, each sampled correlation value is actually the integrated value over a finite area of the correlation plane. Modeling of these two effects to the degree necessary to quantify the performance obtainable is beyond the scope of our present effort.

Another vital issue of concern in this approach is that input plane translation of the object does not affect the autocorrelation. Thus, in-plane shifts of each pattern on the target must be obtained by other methods. It appears possible to obtain such information from the output correlation plane samples. This follows, since input plane translations never occur alone. They are always associated with an input plane rotation (i.e. the entire wing does not shift, rather it rotates about the fuselage and shifts), and in addition, the input object is rigid and hence abrupt changes between adjacent pattern regions on the object are not possible (rather, smoothly varying distortions will result).

To initially address these issues, we used the cross-correlation of two patterns that were shifted by a very small amount. We formed their cross-correlation and sampled it at 5 points (the peak and 2 points on each side of

it). The sampled cross-correlation pattern obtained was sampled with area detectors to model the optical system's detectors. The amount of shift between the two patterns was sub-pixel (i.e. less than the size of one output detector element). For the input pattern, we used a Gaussian-distributed random variable analytical model with known correlation length. We then used a parabolic curve fit of the sampled correlation function and from this obtained a sub-pixel estimate of the shift between the input and reference functions.

In the NTF problem, the pattern used affects the correlation shape function assumed and hence our sub-pixel interpolator model. A parabolic model is often used, but the input pattern should be chosen to properly have such an assumed distribution. The highpass filtering nature of the optical correlator complicates this, since it will change the correlation length of the data and hence the shape of the correlation function. Analysis of all of these issues and quantization of the distortion parameter measurement accuracy obtainable is possible, but does not appear merited since other distortion parameter estimators using simpler feature extractors, simpler post-processing analyses and providing in-plane shift information appear more attractive. An alternative use of this technique that may be preferable is to perform a coarse correlation to determine approximately where the different object patterns are in the input and to then perform a fine zoom correlation (or to use feature extraction techniques) to obtain more precisely the locations and shapes of each object pattern. This coarse preprocessing may be quite attractive for our stereo correlation approach.

3.6 SUMMARY AND CONCLUSION

In this chapter, we have considered the effect of vibrations and turbulence on the resultant processor for the wind tunnel problem. Various candidate schemes have been advanced. None appear to be extremely attractive, except perhaps for time-averaged moire. Recent results obtained by NASA [10] have indicated that the problems associated with turbulence and changes in index of refraction are not too severe and thus can be overcome. We thus do not consider such issues further. Space-variant pattern recognition techniques were considered. They appear to be able to provide the necessary accuracy, however these systems are more complex than others and are thus not considered further.

A new version of stereo correlation processing was advanced. With the modifications which we noted, this technique can be applied to the analysis of object distortions for wind tunnel model testing and to achieving both in-plane and out-of-plane distortion measurements. This technique is likewise capable of achieving the required accuracy. However, again, because of the complexity of the resultant system, it is not considered further.

Finally, a novel and most attractive new approach (analyses of the shape of the autocorrelation of the distorted object pattern) was advanced. This technique also appears to offer significant promise. Its accuracy and the optimum pattern to use remain to be quantified. As before, in-depth analyses and laboratory demonstrations of every possible approach are not possible. Our initial laboratory demonstrations of this technique are quite attractive.

This concept and our stereo scheme merit further attention. Time did not permit this, thus we chose to next investigate various simpler feature extraction algorithms as discussed in the next chapter.

4. OPTICALLY-GENERATED PATTERN FEATURES FOR DISTORTION PARAMETER ESTIMATIONS

4.1 INTRODUCTION

In this chapter, we discuss several coherent optical deformation-measurement techniques that can broadly be classified as feature extraction methods. In all instances, we consider projecting a pattern onto selected regions of the model surface, imaging the deformed pattern (as it appears when projected onto the model) into an optical processor, where it is operated upon to optically extract various image features. By image features, we refer to various scalar quantities that describe the deformed object pattern for different regions of the model. The use of optical processors for feature extraction is very new. The analysis of such features for distortion parameter analysis (rather than for object identification) is thus a very virgin area of research.

For reasons mentioned before, patterns for each object region, rather than simple points on the target are used. The types of patterns considered are discussed in Section 4.2. We consider ten patterns in ten spatially distinct regions along the wing for simplicity and with no loss of generality. If we know (from our feature extraction and processing) the 3-D displacements of these ten local regions of the target, then the continuous distortion function for the entire wing can easily be obtained as a tenth-order polynomial (by solving the resultant set of ten simultaneous equations). If greater than ten points are used, the complexity of the associated extraction of the surface deformations will require solving a much larger set of equations. In this case, various optical matrix-vector processing techniques [11] should be considered. Determining the 3-D displacements of discrete regions of the target at discrete

times appears to be adequate, since we expect the model to deform slowly and continuously (rather than abruptly). The increased space bandwidth product that results by using patterns rather than simpler circular or rectangular shapes was noted earlier.

As the two optically-generated image feature extraction techniques to be considered, we address the use of Fourier coefficients and moments. In Section 4.3, we consider the use of a Fourier coefficient feature space. We also include our initial laboratory experiments and quantitative analyses using such a feature space. In this initial study, emphasis is given to the accuracy of this (and all) techniques and to their practical realization. In Section 4.4, we consider a wedge ring detector (WRD)-sampled Fourier transform feature space. This type of feature space is easily produced optically. It has the advantage of a greatly reduced dimensionality, thus significantly reducing the complexity of the post-processing required. In all of our feature extraction techniques, some form of post-processing is required to extract the deformation parameters of the object. This can take the form of a specific post-detection processor, or an estimator. In Section 4.4, we describe our estimator that we propose to utilize. In Section 4.5, the digital simulation requirements to model this algorithm are discussed. A quite significant resolution, fine sampling and extensive computing time is required to obtain a full quantitative analysis of this approach for the NTF problem. In Section 4.6, we consider a new optical processor that computes the geometrical moments for each pattern in each object region of the target. We also detail how a nonlinear estimator can be used to determine the necessary distortion parameters of each object pattern from the optically-produced image features. In Section 4.7, we provide an initial analysis of the component requirements for such a system,

with attention to mask resolution and mask and detector dynamic range and gray level and noise effects. Initial quantitative results obtained are noted and included. Our summary and conclusions and recommendations for future work in this area are then advanced in Section 4.8.

4.2 PATTERNS USED

The simplest pattern considered was a square-wave grating. This grating is shown in Figure 4.1. The grating is of size a , with the bars of the grating being of width c and with a center-to-center spacing b . It is described mathematically by

$$f(x) = \text{Rect}(x/c) * \sum_i \delta(x - ib) \cdot \text{Rect}(x/a). \quad (4.1)$$

The Fourier transform of this pattern is given by

$$F[f(x)] = F[\text{Rect}(x/c)] \cdot F[\sum_i \delta(x - ib)] \cdot F[\text{Rect}(x/a)]. \quad (4.2)$$

The components of the Fourier transform of this pattern are well-known and easily determined.

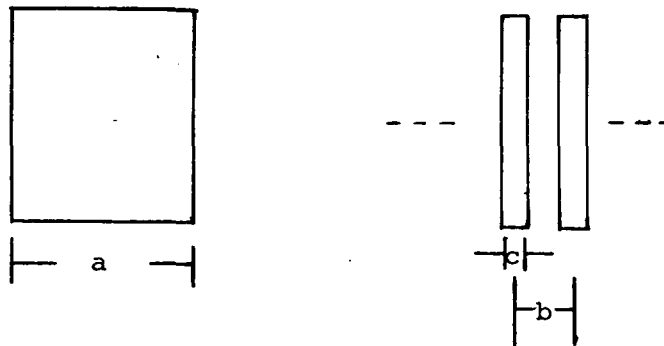


FIGURE 4.1
Simplified Grating Pattern Inputs Used in Analysis

For simplicity, all analyses and experiments were performed with such a grating pattern. Our results can easily be extended to other patterns and cases. Thus, our use of only a 1-D grating represents no loss of generality. The associated post-processing system to extract 3-D deformation information may require more elaborate processing than is required in the presently considered simpler example. A 2-D pseudorandom pattern could also be used, as could 2-D patterns such as Walsh-Hadamard matrices. Such patterns are attractive since they increase the space bandwidth product of each object pattern, help to avoid the presence of cross-correlations between the patterns in different object regions, and should increase the accuracy obtainable in the measured data. If several object patterns are present in the same field of view, or if the location of a given object pattern is not known to sufficient accuracy, the use of 2-D patterns coded such that there is negligible cross-correlation between any two of them can allow us to locate a specific pattern in the input image. Different pseudorandom codes and the Walsh-Hadamard matrices exhibit these desirable very low cross-correlation properties. If the patterns can be placed on the target, different LEDs can be placed behind each (within the target model). These can be pulsed on and used to locate each pattern directly. This latter approach is a distinct possibility. It may prove to be one that can easily be incorporated into a version of the wind tunnel test system that NASA is presently considering fabricating.

As before, we assume that the deformations in each object region are piecewise constant. In Section 4.3, we discuss how the resultant Fourier transform pattern changes with selected simple distortions of the input pattern.

4.3 FOURIER COEFFICIENT FEATURE SPACE

The pattern in the back focal plane P_2 of a lens L_1 is the 2-D Fourier transform of the amplitude transmittance function $f(x,y)$ placed in the front focal plane P_1 . Plane P_2 is located a distance f_L (the focal length of lens L_1) from L_1 . The input plane P_1 can be to the left or right of L_1 . In the system we used in our laboratory tests (see Figure 4.2), plane P_1 is to the right of L_1 and is located a distance d from P_2 as shown in Figure 4.2. This system has less severe lens aberration requirement than does a system with the input pattern placed in front of the transform lens. This system is a scaling Fourier transform processor, in which the scale of the input image (and the resultant Fourier transform that is produced) can be adjusted by simply varying the location of the input object (i.e., varying the distance d in Figure 4.2). The relationship between the location x_2 in P_2 of input spatial frequencies u and the spacing d in Figure 4.2 (and optical system parameters such as the light source used λ and the focal length f_L of the transform lens) is given by

$$x_2 = \lambda du. \quad (4.3)$$

As seen from (4.3), the scale of the Fourier transform plane (or equivalently the scale of the input image) can easily be adjusted by varying the distance d in Figure 4.2. Similarly, the rotational orientation of the input object, and hence the angular location of the spatial frequencies in plane P_2 can also easily be varied by simply rotating the input image in plane P_1 . This experimental system is thus most attractive for producing various input image distortions. It must be modified to accommodate 3-D distortions (unless we simply

view such distortions as scale changes in the input image). This assumption appears to be most valid since 1-D scale changes in the x or y direction are appropriate models of various out-of-plane rotational distortions of the object test pattern. If the image in the input P_1 plane is tilted out-of-plane, then linear phase terms are introduced into the input data. This will cause a shift in the P_2 pattern data recorded as well as a form of 1-D scale change in the input object pattern.

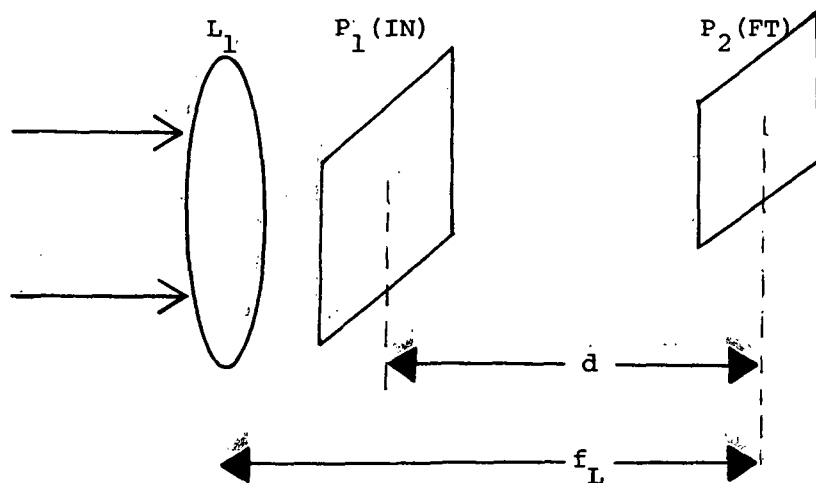


FIGURE 4.2 Simplified Schematic of the Scaling Fourier Transform Processing System.

The P_2 pattern contains diffraction orders separated by

$$x_2 = \lambda d/b \quad (4.4)$$

that are oriented at small angles θ with respect to the axes of P_2 (for an input pattern inclined at an angle θ). The input distortion Δw is proportional to the change Δb in the pitch of the grating. The expected resolution of the system is given by the Fourier transform of the aperture function, specifically by

$$\Delta R = \lambda f_L / a. \quad (4.5)$$

This is the minimum Δb distortion that is measurable with this system.

In our experiments to verify this theory, we used a 100 line pair per inch grating and a Fourier transform lens with focal length $f_L = 760\text{mm}$, He-Ne laser with $\lambda = 633\text{nm}$ and a spacing $d = 650\text{mm}$. We measured the displacement of the various diffracted-order spots in the transform plane for different changes Δd in the distance d in Figure 4.2. By this, we thus simulated different scale changes in the input image. The shift in the location of the n -th diffracted-order thus describes the change Δd (or equivalently an input distortion change Δb) in (4.4). Thus, as a technique to achieve distortion parameter estimation with improved accuracy and performance, we suggest that the location of the higher-order diffracted spots be measured and from their shifts the distortion parameters (e.g., scale change, etc.) be measured. By this new technique (using the n -th diffracted order), we effectively increase the input spatial frequency and hence the shift expected for a given scale change (e.g. a given change in the grating spacing Δb) of the input data pattern. Use of a grating pattern rather than an aperture significantly improves the sensitivity of our measurements.

Our results are summarized in Table 4.1. From these data, we see that a scale change of approximately 0.1% can easily be measured with this system. The measured shifts were compared to those predicted by theory. In all cases, better than 0.5% accuracy was obtained (i.e., we found that we could measure the magnitude of an 0.1% scale change to an accuracy of 0.005%). The accuracy in our present system was limited by the Fourier transform lens used. With a specially-designed Fourier transform lens, better shift linearity is possible. For the present application, the accuracy achieved is sufficient.

For our case of an aperture with $a = 10\text{cm}$, the resolution accuracy of the system is $4\mu\text{m}$ (this is the resolution accuracy in position in the Fourier transform plane). Since a $50\mu\text{m}$ shift in P_2 corresponds to an 0.15% scale change, the present system is capable of measuring scale changes of $(4/50)(0.15) = 4(0.003) = 0.012\%$. This corresponds to a scale change Δb in the grating by $4\mu\text{m}$. This is much better than the requirements dictated for the NTF problem.

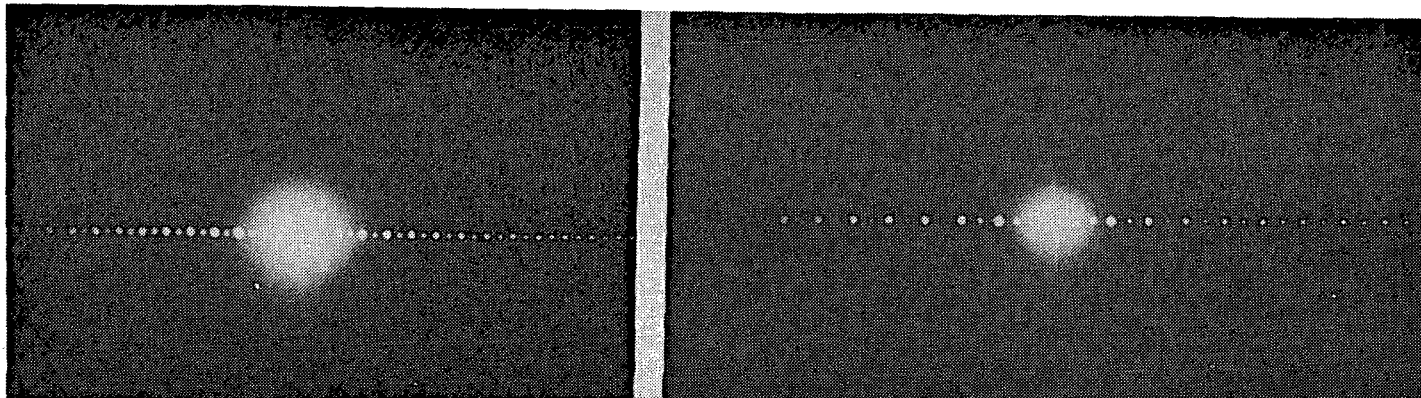
TABLE 4.1

Experimental Data Obtained Using
Fourier Coefficient Measurements

$\Delta d(\text{mm})$	% Scale Change	Observed Shift (20-th order in μm)
65	10%	3207
6.5	1%	330
1	0.15%	51

In Figure 4.3, we show the optically-produced Fourier transforms of the grating in Figure 4.1 using the optical system of Figure 4.2. Figure 4.3a corresponds to one location $d = d_1$ of plane P_1 with respect to plane P_2 . Figure 4.3b corresponds to a $d = d_2$ location of P_1 , corresponding to a scaled or out-of-plane rotated and distorted input image. We clearly see from these patterns that the Fourier transform coefficients occur at spatially different locations in the two cases. From these locations, input scale changes or out-of-plane rotational distortions can be calculated.

ORIGINAL PAGE IS
OF POOR QUALITY



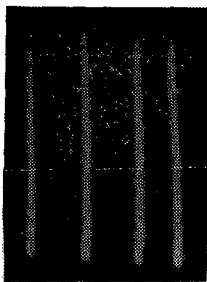
(a)

(b)

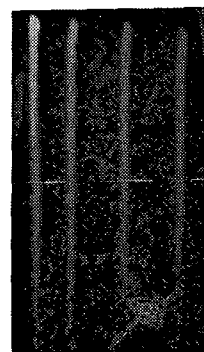
FIGURE 4.3

Partial Fourier Transform Plane Pattern Obtained on the System of Figure 4.2
for Two Distorted Grating Patterns

A cross-sectional scan (obtained with a scanning photometric microscope) of several of the Fourier transform coefficients for the grating Fourier transform pattern in Figure 4.3 are shown in Figures 4.4a and 4.4b for one scale change distortion in the input image. As seen from this data, the higher Fourier transform orders in Figure 4.4b are shifted more to the right than are the corresponding orders in Figure 4.4a. The amount of shift and hence the location of the Fourier transform peaks is proportional the input scale change (i.e. the input distortion) and thus their location provides the desired input pattern distortion data.



(a) No Scale Distortions



(b) Scale Distortions

Figure 4.4

Selected Cross-Sectional Scans of the Fourier Transform Pattern Obtained on
the System of Figure 4.2 With (a) and Without (b) Scale Distortions in
the Input Object Grating Pattern

The sensitivity of this technique is superior to what is obtainable using moire techniques for a given grating spatial frequency. The moire accuracy is simply set by the pitch of the grating (0.25mm for our case). We can achieve significantly better accuracy (by a factor of about 50) by use of our higher-order Fourier transform plane measurement technique. (Fringe multiplication of a projection moire pattern can likewise achieve improved accuracy, however.) Many techniques exist by which the sensitivity of the Fourier transform system can be increased further. These include use of a higher spatial frequency grating and the use of higher grating orders. It is possible to fabricate gratings with strong diffraction orders past the 25th order. Thus, the use of such techniques is quite potentially attractive. Presently, 0.01% scale changes correspond to a tilt of the input object (modeling out-of-plane rotation by θ as a scale change) by $\Delta\theta = 5.7 \times 10^{-3}$ degrees. This is the accuracy of our present system.

However, there are several limitations in this technique that must be noted. This technique is most attractive for measuring input plane distortions such as stress and strain. Such distortions cause the input image $f(x,y)$ to be changed into a new function $f(ax,by)$, where $a = 1 + \epsilon$ and $b = 1 + t\epsilon$ where ϵ is the strain and t is the Poisson coefficient ($t = 0.3$ for many materials). Image plane rotations can also be measured from the angle at which the Fourier transform plane spots occur with respect to the axes of plane P_2 . However, if we use a higher-order Fourier coefficient, then a very large number of Fourier transform plane detectors are required. This is a significant disadvantage of this system. If in-plane rotations can be avoided, and if out-of-plane rotations can be effectively modeled as 1-D scale changes horizontally and vertically, then it should be possible to position a sufficiently sparse detector array at the proper higher-order Fourier coefficient spatial location in the transform plane. This would make this technique quite attractive. In Section 4.4, we describe an alternate technique (with significantly reduced Fourier transform plane dimensionality) that is preferable (if its accuracy is sufficient).

In conjunction with the aforementioned experiments, we also used a fan to produce air turbulence between the input and Fourier transform plane. This was an attempt to model the turbulence present in wind tunnel images. No measured differences were observed in the shape or location of the Fourier transform plane diffracted orders however. Although this experiment is not conclusive, it is promising, since it indicates that such a technique may be less susceptible to air turbulence than are other methods. Other disadvantages associated with a Fourier transform technique (for out-of-plane deformations, which we model above simply as scale changes) is that a large depth of field for the imaging lens which projects the object pattern onto the target will be required. This is necessary to insure that the pattern remains focused on the target over the entire range of deformations to be expected. From discussions with NASA, it appears that cameras with sufficiently large depth of field are available. The use of a pattern behind each laser diode, in a system that NASA is presently considering, appears possible. We also note that the scale changes (or rather the accuracy with which the scale change must be measured) is expected to be quite small. Such small changes can be quite difficult to measure if techniques such as the ones we have proposed are not considered.

4.4 WRD-SAMPLED FOURIER COEFFICIENT FEATURE SPACE CONCEPT

The dimensionality associated with the Fourier transform plane pattern analysis scheme noted in Section 4.3 can become quite excessive. Specifically, the space bandwidth product of an image and its Fourier transform are equal. This, coupled with the various distortion parameters to be investigated can require a significantly large number of detectors for sampling of the Fourier transform space of the object pattern. The digital post-detection analysis

system required for such analysis can also be quite complex, especially when many input samples must be interrogated and linearly combined. As one attractive technique, whereby the dimensionality of such a feature space can be significantly reduced, we consider the use of a wedge ring detector (WRD) to sample the Fourier transform plane.

This device (depicted in Figure 4.5) consists of 32 annular-shaped detector elements in one-half of a one inch silicon detector, with 32 wedge-shaped detector elements in the other half of this detector. Such detector elements exist commercially. They are quite useful and efficient for data-reduction purposes. In the instance that we consider here, we employ them to reduce the dimensionality of the Fourier coefficient feature vector (and to produce Fourier coefficient data with more opportunity for invariance to scale, rotation, and in and out-of-plane displacements). The wedge-shaped detector elements should be most useful for providing angular information on the orientation of the input pattern. They are also invariant to object scale changes. The ring (or annular)-shaped detector elements should be most useful in providing scale change information on the object pattern. They are also invariant to plane rotations of the input object. Thus, as a new approach to distortion-parameter estimation, we suggest the use of a wedge-ring-detector-sampled Fourier coefficient feature space to analyze 2-D object patterns placed at different locations on a target in a wind tunnel.

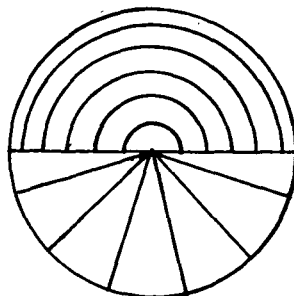


FIGURE 4.5
Pictorial Diagram of the Wedge Ring Detector-Sampling Unit
Proposed for Dimensionality Reduction and Distortion Parameter Estimation.

In conjunction with this reduced dimensionality space concept, we propose the use of a new and unique digital iterative estimator. To understand this concept, we view the 64 WRD-sampled Fourier coefficients produced at the output as the 64 elements of a feature vector $\hat{\underline{v}}$. The purpose of the post-processor is to compare the elements of this observed vector $\hat{\underline{v}}$ with the associated elements $\underline{v}(\underline{b})$ of distorted versions of the reference vector. We denote the distortion parameter vector by \underline{b} . It contains elements such as R (the range or scale of the object pattern), a and b (the horizontal and vertical scale factors), x_0 and y_0 (the horizontal and vertical shifts of the object pattern), and θ and ϕ (the in and out-of-plane rotational angles of the object pattern). Our post-processor begins with an initial estimate of \underline{b} . The elements of $\underline{v}(\underline{b})$ are then computed for this set of distortion parameters. The difference $\hat{\underline{v}} - \underline{v}(\underline{b})$ for this particular choice of \underline{b} is then computed. A new estimate of the parameters of \underline{b} is then obtained, the aforementioned calculations are then repeated, and the procedure repeats until a sufficiently small difference in $\hat{\underline{v}} - \underline{v}(\underline{b})$ is obtained. The iterative algorithm to achieve this is [12]

$$\underline{b}_j = \underline{b}_{j-1} + [\underline{J}^T \underline{\Sigma}^{-1} \underline{J}]^{-1} \underline{J}^T \underline{\Sigma}^{-1} [\hat{\underline{v}} - \underline{v}_i(\underline{b}_{j-1})], \quad (4.6)$$

where \underline{J} is the Jacobian and $\underline{\Sigma}$ is the covariance matrix.

Our initial investigations [12] showed that this algorithm can be realized in fewer than 7 iterations and that each iteration can be computed using less than 6500 operations. By an operation, we refer to a multiplication or an addition. Included in these 6500 operations are 1500 bookkeeping and data management operations. Thus, it appears that this algorithm can be implemented with fewer than 35,000 post-processing operations. It should thus not significantly tax a dedicated digital post-processor. This technique and concept appears most

attractive and we recommend it for future research considerations. A major issue in future research on this concept is an extension of it to 3-D distortions and a quantification of the accuracy and component performance requirements needed. Our initial remarks on these topics are included in Section 4.5.

4.5 INITIAL ISSUES IN THE ANALYSIS OF A WRD/FOURIER-COEFFICIENT FEATURE SPACE

Digital simulation is essential to provide answers to the various issues associated with a WRD-sampled Fourier coefficient feature space and the necessary parameters of our post-detection iterative digital estimator. The object pattern's space bandwidth product required to achieve this prohibits a full analysis of such a subject in our present program effort, even using digital modeling and simulation. To quantify the work required, we first consider the realization of a model of a WRD detector in a digital system. This requires considerable attention to interpolation and area integration. A most important issue associated with such a program is the extension of the aforementioned concept to 3-D image distortions. In such a case, we require a description of the various versions of the object pattern as functions of all parameters associated with a 3-D distortion. This is far more complex than the case noted in Section 4.4. Specifically, consider the case in which out-of-plane rotations occur for object patterns located at different positions on the wing. Even for the case of a fixed out-of-plane rotational angles θ and ϕ (about the fuselage). These correspond to quite different results for each of the different object patterns located at different distances from the fuselage. Thus, 3-D affine transformation matrices are needed to describe the resultant pattern as a function of 3-D distortions. It appears that 3-D distortion data per pattern can be obtained from two images of each pattern taken from different view

angles. This is a vital subject for future research.

4.6 OPTICAL MOMENT FEATURE SPACE SYNTHESIS

As yet another possible optically-generated image feature space, we consider the calculation and use of the moments of an input pattern as the elements of a feature vector. The moments of an input image $f(x,y)$ can be defined as

$$m_{pq} = \iint f(x,y) x^p y^q dx dy. \quad (4.7)$$

Insight into the physical understanding of the various moments is possible (for the lower-order moments). Specifically, the moment m_{00} is the average value of the input image. The moments m_{01} and m_{10} correspond to the centroids of the object in the x and y direction. They thus convey information on the horizontal and vertical displacements of the object in the input plane. The moments m_{02} and m_{20} correspond to the radius of gyration of the object. This has significance and various structural mechanics problems and applications. As a measure of the out-of-plane rotational angle, we can form the ratio of the m_{02} and m_{20} moments. The sine of this angle can be obtained from the sine of any odd-order moment.

Next, we consider an optical processor that is capable of realizing the computation of the moments of an input object pattern in parallel. The simplified version of this system is shown in Figure 4.6. In this figure, the input image $f(x,y)$ is imaged onto a fixed mask, whose amplitude transmittance is described by $g(x,y)$. The light distribution leaving the mask plane is thus the product fg . This pattern is integrated in space to produce

$$u_3 = \iint f(x,y) g(x,y) dx dy \quad (4.8)$$

on an on-axis output plane detector. Comparing this output pattern expression to the expression for the moments, it becomes quite apparent that by the use of various monomial functions for the mask transmittance, the moments of the input image can be produced on the output detector. Specifically, if the mask function is nothing (unity transmittance, i.e. $g(x,y) = 1$), then $u_3 = m_{00}$. If the mask is linearly varying in transmittance in the x direction, i.e. $g(x,y) = x$, or in the y direction, i.e. $g(x,y) = y$, then the observed output plane pattern corresponds to $u_3 = m_{10}$ or $u_3 = m_{01}$ respectively. Extension of this scheme to higher-order moments, using higher-order monomials for the mask, follows directly.

In the recommended version of the system of Figure 4.5, we would spatially-multiplex the various monomial functions onto different spatial frequency carriers and record the composite sum of these on the mask in this system. The output lens is then viewed as a Fourier transform lens. In this case, the output light distribution on a 1-D or 2-D set of output plane detector elements comprises the moments of the input image $f(x,y)$. This architecture is most attractive, since it is capable of generating the moments of an input image in parallel. It is also attractive since the same optical system is capable of computing the moments of any input object pattern. In other words, the optical system (or the mask function) need not be changed if different input images or object patterns are used. In [12], we discussed how the observed output feature vector, \hat{m} (whose elements are the moments of the input object) can be corrected for various possible error sources present in the components of the system. This is a most attractive and practical aspect of this feature extraction system. Specifically, we have found that the output feature vector m need only be multiplied by a fixed matrix to allow it to be corrected for all possible errors in the optical system. In Section 4.7, we discuss the use of such a

optically-generated moment-element feature space for the present NTF distortion parameter estimation problem.

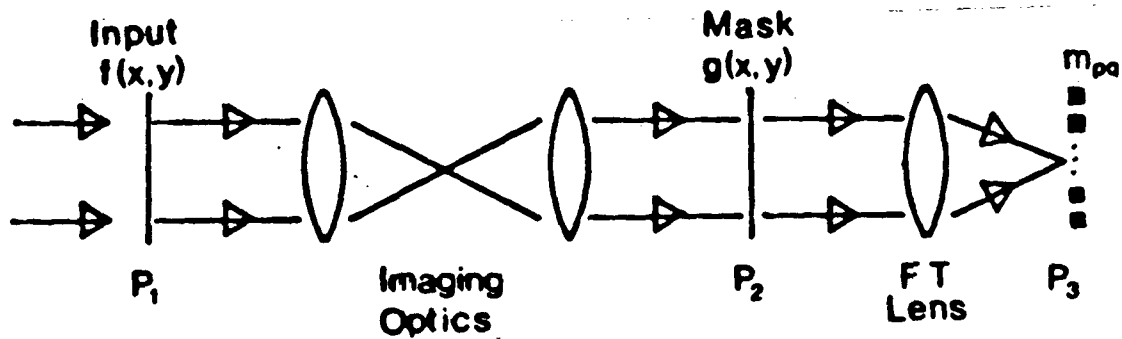


FIGURE 4.6
Schematic Diagram of a Parallel Coherent Optical Processor
to Compute the Moments of an Input Image

4.7 MOMENT PROCESSOR FOR DISTORTION PARAMETER ESTIMATION (COMPONENT REQUIREMENT)

The basic idea in our moment feature space distortion-parameter estimation concept is to compute the moments \hat{m} of each deformed input pattern, compare them to the moments $m(b)$ of the reference object and to then perturb the distortion parameter b as in (4.5) until the weighted distance measure $||\hat{m} - m(b)||^2$ is minimized. The b that minimizes this then describes the distortion parameters for each object pattern region. In this approach, we note that these features can be obtained at different times in the testing of the model within the wind tunnel and that the results can be stored for off-line analysis later. Thus, the required post-processing of the \hat{m} features can be performed off-line. This is quite attractive here, since only 20-25 moments will probably need to be calculated and thus the A/D conversion and storage of 25 scalars per measurement is

ORIGINAL PAGE IS
OF POOR QUALITY

quite easy to achieve. Hence, the high-speed portion of the processing is the computation of the moments and this is what is optically achieved and hence it is quite fast. In the technique that we considered briefly in our present effort, we advance other methods by which the distortion parameters can be computed, directly from the moments, rather than by use of (4.5).

We consider the moments in (4.7) but for the case of a sampled function f_{ij} with a sample size Δw in x and y . Thus, the discrete moments that will be calculated are

$$\begin{aligned} m_{pq} &= \sum_i \sum_j (i\Delta w)^p (j\Delta w)^q (\Delta w)^2 f_{ij} \\ &= w^{p+q+2} \sum_i \sum_j i^p j^q f_{ij}. \end{aligned} \quad (4.9)$$

We consider patterns f_{ij} that are binary and thus set f_{ij} in (4.9) to 1 or 0 for each (i,j) pixel. The summations in (4.9) are from 0 to $N-1$ where N is the number of pixels in the image in x and y . In this case of a binary image, the optical system required is simpler (but also fast digital techniques may be possible).

Let us consider scale and translation distortions (with scale factors A_x and A_y and with translations x_0 and y_0). In the first case, the new moments m'_{pq} of a scaled function are related to the moments m_{pq} of the original undistorted function by

$$m'_{pq} = A_x^{p+q+1} A_y^{p+q+1} m_{pq}. \quad (4.10)$$

In the second case, the new moments m'_{pq} are related to the original moments by

$$m'_{pq} = \sum_i \sum_j \binom{p}{i} \binom{q}{j} x_0^i y_0^j m_{p-i, q-j} \quad (4.11)$$

where i varies from 1 to p and j varies from 1 to q . Similar transformations can be derived in plane rotations, but are not considered here. Out-of-plane rotations by θ are equivalent to a 1-D scale change given by $A = \text{Cos}\theta$. If m'_{pq} and m_{pq} are known for several (p,q) moments, then the distortion parameters (A_x, A_y, x_0, y_0 , etc.) can be obtained using (4.10) and (4.11).

The choice of the test pattern f_{ij} merits future attention. For now, we simply select a square aperture with uniform transmittance of one inside it. This simplifies evaluation and analysis of the equations and reduces recording and lighting effects and requirements. If the images were perfect, if there were no errors in the moment-generating system, and if resolution were infinite, we could evaluate and quantify the differences in the moments for different distorted versions of our input pattern. For now, we note four sources of error and briefly quantify the effects of each.

- (a) The input image has finite resolution, e.g., $N \times N$ pixels ($N = 500$ is typical).
- (b) The recorded monomial will be recorded with finite gray-level resolution Δg , e.g., 500 gray levels.
- (c) The recorded monomial and the carrier each monomial modulates, will be recorded with finite spatial resolution, e.g., $\Delta x = 1\mu\text{m}$ resolution over 1.5cm.
- (d) The optical detector has E levels of detectable values and hence a finite dynamic range, e.g., the moment value will be measured to an accuracy of 1 part in E (1 part in 10^4 is realistic).

Effect (d) limits the minimum moment change and hence the minimum distortion can be measured. For the case when the moments are measured to an accuracy of one part in E, the accuracy to which different distortions can be measured can be determined. For example, for scale distortions, the change in the moments is

$$\Delta m_{pq} = m'_{pq} - m_{pq} = m_{pq} (1 - A_x^{p+q+1} A_y^{p+q+1}) \quad (4.12)$$

and hence the minimum scale distortions must satisfy

$$1/E < 1 - A_x^{p+q+1} A_y^{p+q+1} \quad (4.13)$$

For $E = 10^4$, $p = 3$, $q = 0$ and $A_y = 1$ (no scale change in y), the minimum detector scale change in x that can be measured is

$$A_x \leq 0.999975, \quad (4.14)$$

or one part in 40,000. Thus, excellent accuracy appears possible and this error source does not appear to be significant.

Next, we consider effect (c) of a finite Δx sample size in the monomial mask or the input (effect (a)). Here, we must define an m'_{pq} as a function of Δx and determine if m'_{pq}/m_{pq} as a function of Δx and the order of the moments. Then, we can determine the effect of a given Δx on the measurement accuracy of a given moment. Deriving a general form for this relationship is quite complex. However, for m_{11} , we find, for an $N \times N$ input square pattern

$$m'_{11} = (1/4) [(N+1)/N]^2, \quad (4.15)$$

where $m_{11} = 1/4$. From (4.15), we see that m'_{11} approaches m_{11} as N approaches

infinity. For $N = 500$, the error is 0.4%. Thus, sufficient resolution appears to be possible to produce sufficiently accurate moments to enable measuring the pattern deformations to a quite good accuracy.

Lastly, we consider error source (b). A finite gray-scale resolution $\Delta g = (\text{number of gray levels})^{-1}$ produces a new moment

$$m'_{pq} = m_{pq} + (\Delta x)(\Delta g)M, \quad (4.16)$$

where M is the number of pixels in the pattern (the pattern is again assumed to be of uniform transmittance unity). For 1000 points in each direction and 100 gray levels, 1% error results in the moments m_{00} if the scale changes from 1.0 to 0.75. The effect on other moments can be quantified similarly.

The effect of each of these error sources on the accuracy with which distortions can be measured can be quantified from our initial analysis. This determines the resolution and the dynamic range required in the system. Alternatively, it defines the degree to which different system error sources and noise must be corrected (recall from [12] that the optically-computed moment values can be corrected for various system and noise errors). These are the major issues to be addressed in future work. Our initial analysis summarized above indicates that this feature extraction technique is quite capable of determining distortion parameters and that (4.6) need not necessarily be used to achieve this. This represents a most attractive new approach to object distortion measurements. Clearly, higher-order moments will show higher sensitivity in distortion parameter measurements. A realistic detector dynamic range of 40dB appears to be appropriate. The number of points in the monomial (i.e. its physical size) and the moment order and output SNR are all interrelated. Clearly, physically

larger masks will require more dynamic range. The scale change that results from a $64\mu\text{m}$ change over 7cm (as in the NTF data) will be quite small ($7 \times 10^2 / 64 \times 10^{-6} \cong 10^7$) and thus improved dynamic range will be required (since discrete detectors are used, this appears possible). Since only the edge pixels in the pattern contribute, we can alter the pattern used. Alternately, if a full scale change (from 0.0 to 1.0) is not expected, then the amount of the monomial recorded can be significantly reduced (with an associated reduction in the system's resolution etc. requirements). Similarly, not all moments need to be used (this can significantly reduce the monomial recording requirements). In our future work we plan to quantify these issues, effects, and the accuracy possible with this most attractive technique.

4.8 SUMMARY AND CONCLUSIONS

We find the use of a feature space description of the object pattern at separate locations on the target to be a quite attractive method for distortion parameter estimation. From an analysis of the elements of these feature vectors, and by use of our new iterative estimation algorithm, the distortion parameters associated with the object pattern can be determined. The system architectures we have proposed utilizes the real-time and parallel processing features of coherent optical systems to compute the desired set of image features in parallel. A dedicated post-detection digital processor can then determine the distortion parameters of the object pattern under analysis, with a quite minimal computational load. We recommend that these concepts be pursued and quantified in future research. Both the Fourier coefficient feature space (using a wedge-ring-detector to reduce the dimensionality of the resultant vector) and a moment-based set of image features should be considered.

Both of these features can be optically-generated in the architectures and systems we have described in this chapter. Such an architecture and system represent a simple and most attractive technique for novel applications such as distortion parameter estimation for isolated regions of a deformed target.

5. SUMMARY, HIGHLIGHTS AND FUTURE WORK

Our recent one year of research is summarized in Section 5.1, our major accomplishments are noted in Section 5.2, and future work directions are summarized in Section 5.3.

5.1 SUMMARY

Our brief one year research effort addressing the application of optical data processing techniques to the NTF problem has been quite fruitful. Ten coherent optical data processing techniques were assessed and (following tests on a sample of the target material used in the NTF facility) six additional holographic, moire and speckle pattern techniques were added to our original list. Addressing all sixteen techniques for a new problem and application was a most formidable task. The direction of our research was to survey all methods noted, select the best ones, and for those selected perform laboratory experiments, quantify the accuracy obtainable and define future work directions (to the levels that time permitted).

In Chapter 1, we noted and briefly described all techniques considered, and noted our rationale for omitting many approaches. We also outlined our research and performed initial tests on the diffuseness and specularity of the material used in the NTF facility models. In Chapter 2, we detailed our summary remarks on interferometry, moire and speckle techniques and we performed initial experiments in the most promising areas of research. This included the description of a new moire projection technique coupled with fringe multiplication which has the ability to obtain the desired deformation measurement accuracy. We also suggested several new advanced moire techniques for future research that are

most attractive and appropriate for the NTF application.

In Chapter 3, we addressed several new correlation techniques for optical metrology. We surveyed space-variant techniques and found them to be less attractive than others. We also considered stereo-photogrammetry correlation approaches and found them to be capable of providing sufficiently accurate data and results. We suggested several new applications of this type of approach specifically for the NTF application. The stereo photogrammetry methods are attractive for optical realization, since optical systems easily perform the correlation operation (and since many correlations are required in this approach). We also considered a novel approach to distortion-parameter estimation in which the autocorrelation of a distorted pattern was sampled at only several locations, and from the shape of the resultant correlation pattern, the deformations in the input pattern are extracted. Initial experimental demonstration of this approach was provided and the various areas requiring further attention were noted. This approach requires considerable additional analysis and quantification to determine its appropriateness for the NTF application.

In Chapter 4, new optical feature extraction techniques for the new application of optical metrology were advanced. The use of Fourier transform coefficients and moments (each optically-generated) were given major attention. Initial experimental demonstration of the use of optical Fourier coefficients for distortion-parameter estimation were provided and the various steps needed for future research in this area were noted. A most attractive feature extraction technique, with a considerable dimensionality reduction, involves sampling of the Fourier transform plane pattern using a wedge-ring detector. This approach merits detailed analysis and quantification of the distortion accuracy

possible. The use of optically-generated moments of the input pattern appears to be perhaps the most attractive feature extraction method considered. Our initial quantitative analysis indicates that such a technique can provide adequate distortion-parameter estimates for the NTF application.

Of all of the techniques considered, the projection moire method (with fringe multiplication), the wedge ring detector-sampled Fourier transform technique, and the moment method for determination of pattern distortions appear to be the most attractive ones that merit future detailed attention, quantification, and laboratory demonstration.

5.2 HIGHLIGHTS

The highlights of our one year research effort were:

- (1) Isolation of the major attractive new optical data processing techniques for NTF target surface metrology (Chapter 1).
- (2) Projection moire with fringe multiplication appears capable of the required accuracy and performance (Chapter 2).
- (3) Experimental verification of item (2) was provided (Chapter 2).
- (4) A new moire projection technique was described in which the entire object is illuminated and in which the full distortion parameters of the entire object are obtained at once (Chapter 2).
- (5) A new moire projection technique was described in which deformations rather than object contour is available (Chapter 2).
- (6) Phase conjugate optical techniques were suggested together with video moire methods (Chapter 3).
- (7) Space-variant techniques do not appear appropriate (Chapter 3).

(8) Space-variant pattern recognition techniques appear adequate for some distortions but require a much more complex system than do other approaches (Chapter 3).

(9) Conventional stereo correlation techniques appear to provide sufficient accuracy (Chapter 3).

(10) The use of different object patterns on the target to determine the full object deformation by cross-correlations was suggested (Chapter 3).

(11) A new modified stereo-photogrammetry technique was advanced to achieve object deformation information rather than just object depth data (Chapter 3).

(12) A new modified stereo correlation technique was devised to achieve in-plane and out-of-plane target deformation information (Chapter 3).

(13) An autocorrelation shape analysis method for object distortion measurement was advanced and initial experimental data obtained (Chapter 4).

(14) A new feature extraction technique for distortion-parameter estimation using Fourier transform coefficients was described and initial experimental data obtained (Chapter 4).

(15) A new feature extraction technique for distortion-parameter estimation using wedge ring detector-sampled Fourier transform plane data was described (Chapter 4).

(16) A new feature extraction technique for distortion-parameter estimation using moments was described and initial quantification provided (Chapter 4).

The application of feature extraction techniques to distortion-parameter estimation is a virgin new application area that is significantly different from the conventional pattern recognition and object identification uses previously pursued for feature extraction methods.

5.3 FUTURE WORK

Much future research has been defined as a result of our initial study. These future research topics include:

(1) Further projection moire and fringe multiplication studies, demonstrations and quantification are needed.

(2) Fully detailing, quantifying and demonstrating the full object moire technique we described should be pursued.

(3) Fully detailing, quantifying and demonstrating our contact print moire technique to provide in-plane distortions should be addressed.

(4) Fully detailing, quantifying and demonstrating of our differential moire technique to extract only object distortion information rather than object shape information should be pursued.

(5) Processing of the information on the location of different LED images on different cameras by optical matrix-vector processors merits attention.

(6) Optical correlation, convolution and Fourier transform techniques can aid in the interpretation of the moire contour output patterns produced.

(7) Optical matrix-vector techniques can aid in providing global object distortion information from several spatially-measured distortion values.

(8) Extension of, detailing and quantification of the use of our present stereo-correlation techniques to provide in-plane and out-of-plane 3-D object distortion information merits attention.

(9) Video moire techniques appear to merit initial study.

(10) Phase conjugate optical techniques merit attention if they can be used to correct the medium turbulence present in the NTF application.

(11) The new modified stereo-photogrammetry techniques we advanced to

determine object deformations rather than object depth information and in-plane as well as out-of-plane distortions merit further research.

(12) Wedge ring detector-sampled Fourier transform data is attractive but requires additional analysis by digital simulation.

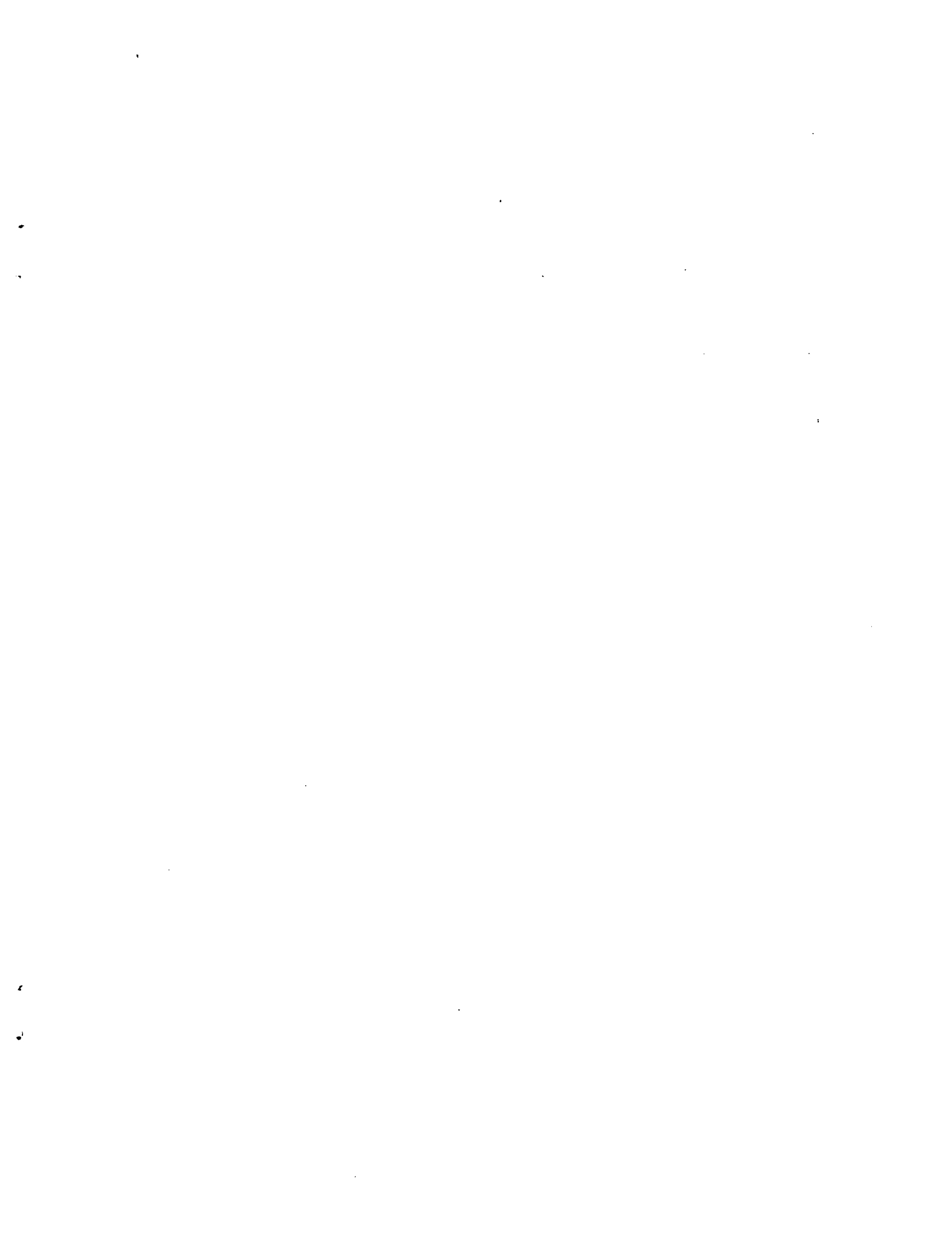
(13) The moment-based feature extraction technique merits future research, quantification and experimental verification.

From the many techniques addressed, studied, suggested and analyzed, the simplest techniques are of course the most attractive ones. For future research, we recommend pursuit of the following three items:

- (A) Projection moire with fringe multiplication.
- (B) Wedge ring detector-sampled Fourier transform feature extraction.
- (C) Moment-based feature extraction.

REFERENCES

1. B. Hildebrand and J. Doty, "A Study of Model Deflection Measurement Techniques Applicable within the National Transonic Facility", NASA CR-165853, February 1982.
2. J. Harris and K. Harding, "Evaluation of Moire Techniques for Wind Tunnel Metrology", NASA CR-164477, June 1981.
3. W. T. Welford, "Some Applications of Projected Interference Fringes", Optica Acta, 16, 371 (1969).
4. D. Meadows et al, "Generation of Surface Contours by Moire Patterns", Applied Optics, 9, 942 (1970).
5. R. Ritter and H. Mayer, "Vibration Analysis of Plates by a Time-Averaged Projection-Moire Method", Applied Optics, 19, No. 5 (1979).
6. B. Hildebrand and J. Doty, "A Study of Model Deflection Measurement Techniques Applicable within the National Transonic Facility", NASA CR-165853, February 1982, pp. 43-50.
7. D. Casasent and D. Psaltis, "New Optical Transforms for Pattern Recognition", Proc. IEEE, 65 (1977). See also D. Casasent and D. Psaltis, "Space Bandwidth Product and Accuracy of the Optical Mellin Transform", Applied Optics, 16, 1472 (June 1977).
8. A. VanderLugt, IEEE, Information Theory, 128 (1964).
9. N. Balasubramanian, Chapter in "Optical Data Processing: Applications", Editor-D. Casasent, Springer-Verlag (1978).
10. D. Post, "Analysis of Moire Fringe Multiplication Phenomenon", Applied Optics, 6, 1938 (1967).
11. C.P. Neuman and D. Casasent, "Optical Systolic Solutions of Linear Algebraic Equations", NASA Langley Research Center, Optical Information Processing Conference II, Hampton, Virginia (August 1983).
12. D. Casasent, L. Cheatham and D. Fetterly, "Optical System to Compute Intensity Moments: Design", Applied Optics, 21, 3292-8 (September 1982).



1. Report No. NASA CR-172316		2. Government Accession No.		3. Recipient's Catalog No.	
4. Title and Subtitle New Coherent Optical Techniques for National Transonic Wind Tunnel Facility				5. Report Date March 1984	
				6. Performing Organization Code	
7. Author(s) David Casasent				8. Performing Organization Report No.	
9. Performing Organization Name and Address Carnegie-Mellon University Department of Electrical Engineering Schenley Park Pittsburgh, PA 15213				10. Work Unit No.	
				11. Contract or Grant No. NAG1-265	
12. Sponsoring Agency Name and Address National Aeronautics and Space Administration Washington, DC 20546				13. Type of Report and Period Covered Contractor Report	
				14. Sponsoring Agency Code	
15. Supplementary Notes Langley Technical Monitor: H. D. Hendricks Final Report - 1 May 1982 - 1 May 1983					
16. Abstract <p>The goal of this 1-year study was to survey the use of optical data processing techniques for distortion-parameter estimation in the National Transonic Facility and to assess, quantify and compare various methods to determine which are best for this specific application. The conventional nondestructive testing techniques studies included interferometry, moire and speckle methods. From these, we find projection moire using fringe multiplication to provide sufficient accuracy and to be a most attractive approach for this application. Several advanced moire techniques for future research are also described. We also investigated several correlation techniques: space-variant processing, stereo correlation and autocorrelation shape analysis. Stereo correlation is found to have sufficient accuracy and new modified stereo correlation techniques for this application which are most appropriate are described. Autocorrelation shape analysis is a quite unique approach to distortion-parameter estimation. Finally, several optical feature extraction techniques were considered. These included Fourier transform coefficients, wedge ring detector-sampled Fourier transform data and moment features. In all cases, each feature is optically-generated and a digital post-processor is used to determine the target's distortion parameters. We find: projection moire (with fringe multiplication), wedge ring detector Fourier transform plane analysis and moment-based optically-generated features to be the most attractive techniques that merit further attention for this application.</p>					
17. Key Words (Suggested by Author(s)) Optical Data Processing Techniques Stereo Correlation Auto Correlation Fourier Transform			18. Distribution Statement FOR U.S. GOVERNMENT AGENCIES AND THEIR CONTRACTORS ONLY		
19. Security Classif. (of this report) Unclassified		20. Security Classif. (of this page) Unclassified		21. No. of Pages 75	22. Price

